THE FASEB JOURNAL

RESEARCH ARTICLE

Hypoxia reveals a new function of Foxn1 in the keratinocyte antioxidant defense system

Sylwia Machcinska[1] | Katarzyna Walendzik[1] | Marta Kopcewicz[1] |
Joanna Wisniewska[1] | Anne Rokka[2] | Mirva Pääkkönen[2] | Mariola Slowinska[1] |
Barbara Gawronska-Kozak[1]

[1]Institute of Animal Reproduction and Food Research, Polish Academy of Sciences, Olsztyn, Poland

[2]Turku Bioscience Centre, University of Turku and Åbo Akademi University, Turku, Finland

Correspondence
Barbara Gawronska-Kozak, Institute of Animal Reproduction and Food Research, Polish Academy of Sciences, Tuwima 10, Olsztyn 10-748, Poland.
Email: b.kozak@pan.olsztyn.pl

Abstract

Skin exposed to environmental threats, including injuries and oxidative stress, develops an efficient but not fully recognized system of repair and antioxidant protection. Here, using mass spectrometry analysis (LC–MS/MS), followed by in vitro and in vivo experiments, we provided evidence that Foxn1 in keratinocytes regulates elements of the electron transport chain and participates in the thioredoxin system (Txn2, Txnrd3, and Srxn1) induction, particularly in a hypoxic environment. We first showed that Foxn1 in keratinocytes upregulates glutathione thioredoxin reductase 3 (Txnrd3) protein expression, and high levels of *Txnrd3* mRNA were detected in injured skin of Foxn1$^{+/+}$ mice. We also showed that Foxn1 strongly downregulated the Ccn2 protein expression, participating in epidermal reconstruction after injury. An in vitro assay revealed that Foxn1 controls keratinocyte migration, stimulating it under normoxia and suppressing it under hypoxia. Keratinocytes overexpressing Foxn1 and exposed to hypoxia displayed a reduced ability to promote angiogenesis by downregulating Vegfa expression. In conclusion, this study showed a new mechanism in which Foxn1, along with hypoxia, participates in the activation of antioxidant defense and controls the functional properties of keratinocytes.

Abbreviations: Ad-Foxn1, Foxn1-eGFP-expressing adenovirus; Ad-GFP, GFP-expressing control adenovirus; Amotl2, angiomotin-like protein 2; BrdU, bromodeoxyuridine; CCN1/CYR61, cellular communication network factor 1 /cysteine-rich protein 61; CCN2/CTGF, cellular communication network factor 2 /connective-tissue growth factor; DFs, dermal fibroblasts; Egfr, epidermal growth factor receptor; Ep300, histone acetyltransferase p300; ETC, electron transport chain; Fih-1, factor inhibiting Hif-1α; Foxn1, Forkhead box N1 transcription factor; GFP, green fluorescent protein; Glrx5, glutaredoxin-related protein 5; Grxs, Glutaredoxins; GSH, glutathione; Hif1-α, hypoxia inducible factor1-alpha; HUVEC, human umbilical vein endothelial cells; Ker, keratinocytes; LC-MS/MS, liquid chromatography with tandem mass spectrometry; Ndufa2, NADH dehydrogenase [ubiquinone] 1 alpha subcomplex subunit 2; Ndufa13, NADH dehydrogenase [ubiquinone] 1 alpha subcomplex subunit 13; Ndufb1, NADH dehydrogenase [ubiquinone] 1 beta subcomplex subunit 1; Ndufb4, NADH dehydrogenase [ubiquinone] 1 beta subcomplex subunit 4; Ndufb5, NADH dehydrogenase [ubiquinone] 1 beta subcomplex subunit 5; Ndufv2, NADH dehydrogenase [ubiquinone] flavoprotein 2; Nqo1, quinone dehydrogenase NAD(P)H1; Pdpk1, phosphoinositide-dependent kinase-1; Plcd1, 1-phosphatidylinositol 4,5-bisphosphate phosphodiesterase delta-1; Prx, peroxyredoxin; Romo1, reactive oxygen species; ROS, reactive oxygen species; Srxn1, sulfiredoxin 1; Txn1, thioredoxin 1; Txn2, thioredoxin 2; Txnrd1, thioredoxin reductase 1; Txnrd2, thioredoxin reductase 2; Txnrd3, Glutathione thioredoxin reductase 3; Vdac1, voltage-dependent anion-selective channel 1; VEGF, vascular endothelial growth factor; Yap1, yes1 associated transcriptional regulator.

1 | INTRODUCTION

The skin, as the outermost barrier of the body, is exposed to threats from the external environment including injuries, oxidative stress caused by pollutants, xenobiotics, and UV irradiation.[1,2] Therefore, efficient systems of repair and antioxidant protection of damaged skin that are achieved by an extraordinary mechanism involving the interaction of cells, cytokines, and growth factors are vital for survival.[2–5] The skin wound healing process is characterized as a series of sequentially overlapping phases, for example, inflammation, proliferation, and remodeling, resulting in scar formation.[3,6] Keratinocytes, as the major cell type constituting the epidermis, play numerous roles essential for skin repair.[7,8] One of the most prominent events is re-epithelialization, whereby keratinocytes migrate, proliferate, and differentiate to restore the epidermal barrier.[8,9] These processes are regulated by transcription factors such as AP-1, Pparβ/δ, Foxo1, and Foxn1, which synchronize their downstream gene expression. However, the precise interactions between transcription factors and their regulatory networks are still unclear and await clarification.[10–13]

The transcription factor Foxn1 (Forkhead box protein N1) has been recently recognized as a key regulator involved in skin wound healing.[13,14] Expression of Foxn1 in the skin has been detected in the epidermis and in hair follicles. It has been documented that in noninjured skin, Foxn1 regulates the balance between the proliferation and differentiation of keratinocytes, stimulating proliferation through cell–cell contact and paracrine secretion.[15–17] Furthermore, during the skin wound healing process, Foxn1 is involved in re-epithelialization.[13,14] Evidence exists that Foxn1 is a major activator of several keratin and keratin-associated genes.[18,19] Potter et al. showed that hair keratin/keratin-associated protein genes are regulated through Hoxc13/Foxn1 cascade.[19] Nevertheless, the broad phenotypic spectrum of Foxn1 deficiency (nude mice) indicates several Foxn1 target genes awaiting recognition.[20,21]

One of the crucial environmental cues that triggers the wound healing process is acute hypoxia.[22] Hypoxia-inducible factor-1 alpha (Hif-1α) is a master regulator of oxygen homeostasis, which contributes to the wound healing process. The transcription factor Hif-1, a heterodimer composed of two subunits, Hif-1α and Hif-1β, regulates a number of essential pathways in the adaptive responses of cells to hypoxic conditions.[23,24] However, nuclear localization is not sufficient for transcriptional activation by Hif-1α. Hif-1α requires a C-terminal transactivation domain to generate a functional form that recruits the binding protein (CBP)/p300 coactivator protein.[25] Under normoxia, Hif-1α undergoes proteasomal degradation catalyzed by Hif prolyl-4-hydroxylases and factor inhibiting Hif-1 (Fih-1) in an O_2-dependent manner.[22] Hypoxia during skin wound healing stimulates proliferation, migration, and angiogenesis.[26,27]

However, it has also been shown that a hypoxic environment in the skin is associated with oxidative stress.[1] Many reports have indicated that an oxygen-reducing environment affects the stabilization of Hif-1α, especially by acting on thioredoxin 1 (Txn1) activity.[23,28,29] Thioredoxins (Txns) are the major cellular proteins that play crucial roles in the regulation of numerous biochemical processes, especially in maintaining cellular redox homeostasis and cell survival.[30–32] The Txn system includes Txns, thioredoxin reductase (Txnrd), nicotinamide adenine dinucleotide phosphate (NADP), and Txn-interacting proteins.[29,33] Currently, two isoforms of Txns have been identified in mammalian cells: cytosolic Txn1 (12 kDa) and mitochondrial Txn2 (15.5 kDa). The Txnrds include Txnrd1 and Txnrd2.[29,34,35] The third recently identified isoform of Txnrd, Txnrd3, still awaits recognition of its precise role, for example, in the skin wound healing process.[36,37] A properly functioning Txn system protects the cell against oxidative stress, regulates cell proliferation and apoptosis, and participates in signal transmission by regulating the activity of transcription factors.[4,38]

Multiple molecular and cellular mechanisms regulate post-injury skin healing, including the migratory and proliferative properties of keratinocytes. Defects in keratinocyte migration and proliferation cause incorrect healing.[8] The CCN protein family (Cyr61/CTGF/NOV), including CCN 1–6, a complex of multifunctional proteins, contains proteins that are involved in many important biological functions, including cell proliferation, angiogenesis, tumor formation, and wound healing.[39,40] The best-known proteins that are involved in skin wound healing are matricellular proteins: CCN1 (cysteine-rich protein 61 CYR61) and CCN2 (CTGF connective-tissue growth factor), which are strongly expressed in the epidermis and hair follicles.[41–43] CCN1 in the skin is involved in the regulation of inflammation, cell adhesion, angiogenesis, and apoptosis,[42] whereas CCN2 expression is transiently upregulated after dermal injury to regulate cell adhesion, migration, proliferation, and angiogenesis.[41,44]

Our recent study in which we compared skin gene expression between Foxn1$^{-/-}$ and Foxn1$^{+/+}$ mice through next-generation high-throughput DNA sequencing revealed significant differences associated with reduced oxygen availability: Hif-1α and Txns.[21] A subsequent study in which we applied in vivo and in vitro approaches identified the transcription factor Foxn1 as a potential regulator of Hif-1α stability during cutaneous wound healing.[45] In the present study, using mass spectrometry (LC–MS/MS)-based proteomics analysis, followed by functional assays, we aimed to identify a possible mechanism by which Foxn1 and/or hypoxia regulate physiological changes in keratinocytes at the molecular and functional levels.

2 | MATERIALS AND METHODS

2.1 | Animals

The in vivo studies were performed on mature, 4- to 6-month-old Foxn1$^{-/-}$ (CBy.Cg-Foxn1/cmdb) and genetically matched Foxn1$^{+/+}$ (Balb/c/cmdb; control) mice that were housed in individually ventilated cages (IVCs) in a temperature (22°C) and humidity (55%) controlled room with a 12-h light/12-h dark cycle at the Center of Experimental Medicine (CEM), Medical University of Bialystok, Poland.

Keratinocytes and dermal fibroblasts (DFs) for in vitro studies were isolated from newborn Foxn1$^{+/+}$ (C57BL/6J mice; keratinocyte isolation) and 8- to 11-week-old Foxn1$^{-/-}$ mice (CBy. Cg-Foxn1 <nu>/cmdb; DF isolation). Mice were bred and housed in a temperature- and humidity-controlled room (22 ± 2°C and 35%–65% humidity) with a 12-h light/12-h dark cycle at the Institute of Animal Reproduction and Food Research, Polish Academy of Sciences, Olsztyn, Poland.

The experimental animal procedures were approved by the Ethics Committee of the University of Warmia and Mazury (Olsztyn, Poland), No. 68/2018. The study was carried out in accordance with EU Directive 2010/63/EU of the European Parliament and of the Council on the Protection of Animals Used for Scientific Purposes (OJEU, 2010. Official Journal of the European Union. Directive 2010/63/EU of the European Parliament and of the Council on the protection of animals used for scientific purposes. OJEU. [cited 2010 Oct 20]; Series L 276:33–79).

2.2 | Wound model

The day before the experiment, Foxn1$^{+/+}$ mice were anesthetized with isoflurane, and the dorsal area was shaved and rinsed with an alcohol swab. The next day, Foxn1$^{+/+}$ and Foxn1$^{-/-}$ mice were anesthetized with isoflurane, and a sterile 4-mm diameter biopsy punch (Miltex) was used to create four excisional wounds on the backs of the mice. Excised skin samples (4 mm in diameter) were collected, frozen in liquid nitrogen, and stored at −80°C until analysis (Day 0, uninjured control). After wounding, the mice were placed in cages until recovery. Skin samples were collected postmortem with an 8 mm biopsy punch on Days 1, 3, 5, 7, 14, and 21 after wounding ($n = 6$ animals per group, per time point). Excised, wounded skin tissues were frozen in liquid nitrogen for protein and RNA isolation. Samples for histological examination were fixed in 10% formalin (FA) (Sigma-Aldrich Co.).

2.3 | Cell isolation and culture

DFs were isolated from the excised skin of Foxn1$^{-/-}$ mice that were subjected to enzymatic digestion in collagenase type I (3.68 mg/ml; Sigma-Aldrich Co.) for 80 min at 37°C in an incubator shaker and filtered through 100 μm strainers. The cells were centrifuged for 5 min at 1200 rpm at room temperature. The cells were plated in 60 mm Petri dishes in DMEM/F-12 medium (Sigma-Aldrich Co.) with 15% fetal bovine serum (FBS, Life Technologies, Thermo Fisher Scientific) and gentamicin/amphotericin solution (Life Technologies, Thermo Fisher Scientific). Confluent fibroblasts were trypsinized (0.05%; Sigma-Aldrich Co.) and frozen for further experiments.

Keratinocytes were isolated from the skin of newborn Foxn1$^{+/+}$ mice. Collected skin samples were incubated in dispase (6 U/ml; Life Technologies, Thermo Fisher Scientific) overnight at 4 °C. The separated epidermis was digested in 0.05% trypsin–EDTA (Life Technologies, Thermo Fisher Scientific) for 3 min and filtered through a 70 μm strainer (Falcon, A Corning Brand). Then, keratinocytes were collected by a series of three trypsin digestions (at 37°C), filtered, and centrifuged at 1200 rpm for 5 min at room temperature. The cells were suspended and seeded in DMEM/F-12 medium (Sigma-Aldrich Co.) with 10% FBS (Life Technologies, Thermo Fisher Scientific), 0.2% Primocin (InvivoGen), and 120 μM β-mercaptoethanol (Sigma-Aldrich Co.). The media were changed to keratinocyte-specific medium (CellnTec) 24 h after seeding.

2.4 | Keratinocyte-DFs co-culture for proteomics experiments

Keratinocytes seeded in inserts (Corning® BioCoat™ Control Inserts with 0.4 μm PET Membrane) at densities of 1.3×10^6 after reaching 70% confluency were

transduced with Foxn1-GFP-expressing (Ad-Foxn1) or control (Ad-GFP) adenoviruses.[41] After 4 h, 1 ml of CnT basal medium with supplements A, B, and C (CELLnTEC) was added per insert. DFs ($p = 1$) were seeded in 6-well plates (Corning Falcon) at a density of 0.3×10^6 cells per well. For co-culture experiments, keratinocytes (cultured in inserts) and DFs (cultured on the bottoms of 6-well plates) were set up together and cultured under normoxic (21% O_2) or hypoxic (1% O_2) conditions for 24 h.

2.5 | KCM collection and preparation for proteomic analysis

Conditional medium (KCM) collected from keratinocytes transduced with Ad-Foxn1 or Ad-GFP and co-cultured with DFs for 24 h under normoxic or hypoxic conditions was centrifuged at 300 g for 10 min at 4°C, filtered, and stored frozen at −80°C for further analysis.

Frozen KCMs were thawed on ice and transferred to a new Falcon tube. After gentle mixing of the conditioned medium, 2% sodium deoxycholate solution was added (v/v) (Thermo Fisher Scientific) and incubated on ice for 30 min. After incubation, trichloroacetic acid (Sigma-Aldrich Co.) was added to each tube (gently mixing) to a final concentration of 7.5% (v/v) and incubated again on ice for 60 min. Precipitated proteins were collected by centrifugation at 15 000 g for 20 min at 4°C, and the supernatants were discarded. Next, 20 ml of 100% ice-cold (−20°C) acetone was added, and the pellets were vortexed until the precipitate was dissolved, followed by 10 min incubation at −20°C. After centrifugation (15 000 g for 5 min at 4°C), the supernatants were discarded, and the wash of the protein pellets was repeated twice with 5 ml of 100% ice-cold (−20°C) acetone. The pellets were air-dried for 10 min and dissolved in 2% SDS and 50 mM Tris–HCl (pH 7.55; Sigma-Aldrich Co.). The protein concentration was determined by the BCA method (Thermo Fisher Scientific).

2.6 | Keratinocyte collection and preparation for proteomics analysis

Keratinocytes transduced with Ad-Foxn1 or Ad-GFP and co-cultured for 24 h with DFs under normoxic and hypoxic conditions ($n = 3$, total $n = 6$ animals) were washed with cold PBS. Then, lysis buffer (2% SDS, 50 mM Tris–HCl pH 7.55; Sigma-Aldrich Co.) with protease inhibitor cocktail (Sigma-Aldrich Co.) was added, and the cells were incubated for 10 min on ice. Adherent keratinocytes were scraped off from the dish with a plastic cell scraper, and the cell suspension was transferred into a precooled microcentrifuge tube for further sonication (3 × 20 s,

20 kHz; with Vibra-Cell VCX 130 PB sonicator). The cell lysates were incubated for 45 min on ice and centrifuged at 10 000 g for 15 min at 4°C. The supernatant was transferred to new tubes, and the protein concentrations were measured using the standard Bradford protocol (Bradford Reagent, Sigma-Aldrich Co.). Cell lysates were stored frozen at −80°C for further experiments.

2.7 | S-Trap micro column protocol

Proteins isolated from keratinocytes and conditioned medium samples were thawed, and DNA was sheared by 5 min probe sonication with 30 s on/off cycles. Samples were clarified by centrifugation for 10 min at 16 000 g. All proteins from the conditioned medium samples (ranging from 8.6 to 20.8 μg of proteins in volume of ~100 μl) and 25 μg from cell lysate samples were taken for trypsin digestion with S-Trap micro columns (ProtiFi). The volume of the samples was adjusted to 150 μl with 2% SDS in 100 mM triethylammonium bicarbonate (TEAB), pH 7.1. Conditioned media and cell lysate samples were reduced with 5.5 mM or 9.5 mM 1,4-dithiothreitol (DTT) in 100 mM TEAB and incubated at 37°C for 1 h. Conditioned media and cell lysate samples were alkylated with 25 mM or 37 mM iodoacetamide (IAA) in 100 mM TEAB, respectively. The samples were incubated at room temperature (RT) for 1 h. The reaction was quenched by the addition of 25 mM or 36 mM DTT to the conditioned media and cell lysate samples, respectively. Aqueous phosphoric acid was added to all samples at a final concentration of 1.2%. Six volumes of 90% methanol (MeOH) in 100 mM TEAB, pH 7.1, were added to all samples. The samples were loaded on S-Trap micro columns and centrifuged at 4000 g until all samples had passed through the column. This step was repeated once. Captured proteins were washed four times with 150 μl of 90% MeOH in 100 mM TEAB, pH 7.1. Proteins of the conditioned media and cell lysate samples were digested in 20 μl of 50 mM ammonium bicarbonate solution containing 1 or 1.5 μg of sequencing grade modified trypsin (Promega), respectively. The samples were incubated for 2 h at 47°C. Peptides were eluted in three steps. Each step was followed by centrifugation at 4000 g. First, 40 μl of 50 mM ammonium bicarbonate solution was added, and the solution was incubated for 30 min before peptide elution. Then, 40 μl of 0.2% aqueous formic acid was added to the samples, and hydrophobic peptides were eluted with 35 μl of 50% acetonitrile containing 0.2% formic acid. Recovered peptides were evaporated to dryness in a SpeedVac (Thermo Fisher Scientific).

Before mass spectrometry (MS) analysis, the digested peptides were reconstituted to 0.1% formic acid, and peptide concentrations were determined with a NanoDrop

One spectrophotometer (Thermo Fisher Scientific). For retention time calibration, samples were spiked with iRT-peptides (Biognosys AG) at a ratio of 1:60 for dermal fibroblast cell lysate samples and at a ratio of 1:40 for all the other samples. For MS analysis, 400 ng of peptides from each conditioned media sample and 500 ng peptides of each cell lysate sample were taken.

2.8 | Protein analysis by LC–MS/MS

Relative protein quantitation was determined by the data-independent acquisition (DIA) MS method. The LC–MS/MS analyses were performed on a nanoflow HPLC system (Easy-nLC1200, Thermo Fisher Scientific) coupled to an Orbitrap Fusion Lumos mass spectrometer (Thermo Fisher Scientific) equipped with a nanoelectrospray ionization source. Peptides were first loaded on a trapping column and subsequently separated inline on a 15 cm C18 column (75 μm × 15 cm, ReproSil-Pur 5 μm 200 A C18-AQ, Dr. Maisch HPLC GmbH, Ammerbuch-Entringen, Germany). The mobile phase consisted of water with 0.1% formic acid (solvent A) and acetonitrile/water (80:20 [v/v]) with 0.1% formic acid (solvent B). Peptides were eluted with a linear two-step gradient. For conditioned media samples, an 80 min gradient was used. First, a 60 min step from 5% to 21% solvent B, followed by a 20 min step from 21% to 36% solvent B and a wash with 100% solvent B at the end of the method were used. For more complex cell lysate samples, a 120 min gradient was used (90 min from 5% to 21% solvent B, 30 min from 21% to 36% solvent B, followed by a wash stage with 100% solvent B). MS data were acquired automatically by Thermo Xcalibur 4.1 software (Thermo Fisher Scientific). A DIA duty cycle contained one full scan (400–1000 m/z) and 40 DIA MS/MS scans covering the mass range of 400–1000 m/z with variable isolation widths.

2.9 | Data analysis parameters

Data processing was carried out by Spectronaut 14.3. software (Biognosys AG, Switzerland). A library-free directDIA analysis was performed with a FASTA file of *Mus musculus* (SwissProt, 5.12.2019). Carbamidomethyl (C) was used as a fixed modification, and acetyl (protein N-term) and oxidation (M) were used as variable modifications. The *p*-value was calculated as the inverse cumulative distribution function of the decoy distribution for a given discriminant score (Spectronaut Cscore). The protein and precursor identification *q*-value (multiple testing corrected *p*-value) cutoff was set to .01. Quantification was based on peak area and was carried out at the MS2 level.

Proteins with a *q*-value below or equal to 0.05 and an absolute log2 ratio above 0.58 were considered significantly differentially expressed.

2.10 | Gene ontology and bioinformatics analyses

Gene ontology (GO) annotation of differentiated proteins was performed by using online bioinformatics tools of PANTHER (Protein Analysis Through Evolutionary Relationships).

Classification System, version 16.0 (released 2021–05; https://pantherdb.org/),[46] enriched with the g: Profiler database.[47] The Kyoto Encyclopedia of Genes and Genomes (KEGG) was used for annotation of biological pathways involved in the cellular response to Ad-Foxn1 versus Ad-GFP transduction and hypoxia versus normoxia conditions.[48,49] The analysis of potential protein–protein interactions was performed with the Search Tool for the Retrieval of Interacting Genes (STRING) online database, version 11.0 (https://string-db.org)[50] with a medium confidence score cutoff of 0.4. Protein–protein interaction networks were constructed using Cytoscape software (Cytoscape.org), version 3.8.2.[51] A heatmap containing Foxn1-enriched proteins under hypoxic or normoxic conditions was created using GraphPad Prism Version 9.0 (GraphPad Software, La Jolla, CA, USA). To identify the Foxn1 transcription factor binding sites/motif within the thioredoxin system (Txn1, Txn2, Txnrd1, Txnrd2, and Txnrd3), TSS profiles were extracted for the promoter regions ranging from −3000 bp to +200 bp relative to TSS using EPD-Eukaryotic Promoter Database.[52] The specified region was scanned for matches to the Foxn1 binding site (GACGC)[53] at cutoff *p*-value ≤.01 or *p*-value ≤.001 using FIMO within MEME Suite 5.4.1.[54,55]

2.11 | Keratinocyte functionality analysis

2.11.1 | Cell metabolic activity (MTT) measurement

Keratinocytes isolated from newborn Foxn1$^{+/+}$ mice ($p = 0$, $n = 5$ each in triplicate) were seeded in 24-well plates at a density of 3×10^5 cells/well. At 50%–60% confluency, keratinocytes were transduced with Ad-Foxn1 or Ad-GFP and cultured for 24 h under hypoxic or normoxic conditions. Then, metabolic activity was measured based on a modified MTT (3-[4,5-dimethylthiazol-2-yl]-2,5-diphenyltetrazolium bromide; Sigma-Aldrich Co.) colorimetric method. In brief, 10 μl of sterile MTT solution (5 mg/ml) was added to each well and incubated

for 4 h (normoxia or hypoxia). After incubation, the medium was removed, and formazan crystals were dissolved in 100 μl of DMSO within 30 min in an incubator (37°C) with gentle shaking (30 rpm). Absorbance was measured at 570 nm using a microplate reader (Multiskan Sky Microplate Spectrophotometer, Thermo Fisher Scientific).

2.11.2 | Cell proliferation (BrdU) assay

Flow cytometry was performed on keratinocytes isolated from newborn Foxn1$^{+/+}$ mice ($p = 0$) seeded in 6-well plates at a density of 1×10^6/well. After the cells reached 50%–60% confluency, keratinocytes were transduced with Ad-Foxn1 or Ad-GFP and then cultured under hypoxic or normoxic conditions. After 8 h of incubation, 10 μl of BrdU (1 mM) was added to each well, and the cells were incubated for the next 16 h. Then, the cells were trypsinized (0.05% trypsin–EDTA; Life Technologies), suspended in Dulbecco's modified Eagle's medium (DMEM/F-12; Sigma-Aldrich Co.) with 15% fetal bovine serum (FBS; Life Technologies) and 1% antibiotics (penicillin/streptomycin, Sigma-Aldrich Co.) and counted in automatic counts (Countess II, Invitrogen by Thermo Fisher Scientific). Next, the cells were centrifuged at 1200 rpm for 5 min at RT and suspended in warm sterile PBS. The assay procedure was performed according to the manufacturer's protocol [BD Pharmingen BrdU Flow Kit, Becton Dickinson Cat# 559619 (FITC)]. The labeled cells were analyzed using a BD LSRFortessa Cell Analyzer flow cytometer (Becton Dickinson) and BD FACSDiva v6.2 software (Becton Dickinson). The data are expressed as the percentage of BrdU-positive cells per gated cell.

2.11.3 | Migration assay

Keratinocytes isolated from newborn Foxn1$^{+/+}$ mice were seeded in 12-well plates at a density of 0.6×10^6 per well ($n = 4$; each in duplicate). At 50%–60% confluency, keratinocytes were transduced with Ad-Foxn1 or Ad-GFP. For prevention of cell proliferation, keratinocytes were incubated for 3 h with mitomycin C (10 μg/ml) in CnT medium with supplements A, B, and C (CELLnTEC). The cell monolayers were wounded by scratching a straight line throughout the center of the entire 12-well plate with a 200-μl pipette tip. Debris was removed by washing the cells with PBS, and then, CnT medium with supplements was added. Images were captured with an Olympus microscope (IX51) equipped with an Olympus digital camera (XC50) and analyzed with ImageJ (SciJava software,

National Institutes of Health; NIH). Three representative images of scratched areas were photographed, and the distances between scratched edges were measured. The distance at 0 h was considered to be 100%. The scratched areas were monitored until closure (at 0, 3, 6, 20, 24, and 30 h time points).

2.11.4 | Angiogenesis assay

2.11.4.1 | *KCM collection for angiogenesis*

Keratinocytes isolated from the skin of newborn Foxn1$^{+/+}$ mice were seeded in 6-well plates (Corning, Falcon) at a density of 1.3×10^6. At 70% confluency, keratinocytes were transduced with Foxn1-GFP-expressing (Ad-Foxn1) or control (Ad-GFP) adenoviruses. After 4 h, 1.6 ml of CnT basal medium with supplements A, B, and C (CELLnTEC) was added to each well, and then, keratinocytes were cultured for 24 h under normoxic or hypoxic conditions. After 24 h of culture, KCM-hypoxia Ad-Foxn1, KCM-hypoxia Ad-GFP, KCM-normoxia Ad-Foxn1, or KCM-normoxia Ad-GFP were harvested and stored frozen at −80°C for further keratinocyte functionality experiments.

HUVECs ($p = 2$; ScienCell Research Laboratories, inc.) were seeded at 1.0×10^6 viable cells in a T25 cell culture flask (Corning, USA) in endothelial cell growth basal medium-2 (EBM™-2) with supplements (Clonetics®, Lonza, Verviers). After 3 days of culture, confluent cells were starved in EBM™-2 medium with 0.5% FBS for 1 h. Detached by trypsinization (0.05%; Sigma-Aldrich Co.), cells were seeded ($p = 2$; $n = 5$ replicates) at 2.5×10^4 viable cells/well in a μ-Plate Angiogenesis 96-well plate (Ibidi GmbH) coated with 10 μl of Geltrex™ Reduced Growth Factor Basement Membrane (Gibco, Life Technologies Corporation) per well. Cells were incubated with KCM: KCM-hypoxia Ad-Foxn1, KCM-hypoxia Ad-GFP, KCM-normoxia Ad-Foxn1, or KCM-normoxia Ad-GFP diluted 1:1 with EBM™-2. CnT medium (CELLnTEC) diluted 1:1 in EBM™-2 and supplemented with 1% penicillin/streptomycin was used as a control. Images depicting tube formation were obtained using a Zeiss Axio Observer. Z1 (Carl Zeiss Microscopy GmbH) microscope equipped with ZEN2.6 (Blue edition) software (Carl Zeiss Microscopy GmbH). The formation of capillary-like structures was monitored at 0, 6, 12, and 18 h time points. Images were analyzed with CellSens Dimension software (Olympus Corporation, Tokyo, Japan) with a TruAI neural network module (Olympus Corporation, Tokyo, Japan). The neural network was executed to assess the number of loops and their area (μm^2) per image. Based on their size, loops were divided into three groups, namely, small (2000–10 000 μm^2), medium (10 000–50 000 μm^2), and large (>50 000 μm^2).

2.12 | RNA isolation and quantitative reverse transcription PCR

Quantitative reverse transcription PCR (RT-qPCR) was performed as described previously.[45] Total RNA was isolated using TRIzol Reagent (Invitrogen, Thermo Fisher Scientific). RNA (500 ng) was reverse transcribed with the High-Capacity cDNA Reverse Transcription Kit with RNase Inhibitor (Applied Biosystems, Thermo Fisher Scientific) according to the manufacturer's instructions.

The mRNA levels of *Foxn1* (Cat# Mm01298129), Ker 10 (Cat#Mm03009921_m1), Ker 14 (Cat#Mm00516876_m1), *Txn1* (Cat# Mm00726847_s1), *Txnrd1* (Cat# Mm00443675_m1), *Txn2* (Cat#Mm00444931_m1), *Txnrd2* (Cat# Mm00496766_m1), *Txnrd3* (Cat# Mm00462552_m1), *Vegfa* (Cat# Mm00437306_m1), and *Ep300* (Cat# Mm00625535_m1) were measured. Single Tube TaqMan Gene Expression Assays (Life Technologies Thermo Fisher Scientific) were used. Hypoxanthine phosphoribosyltransferase 1 (*Hprt1*, Cat# Mm01545399_m1) was chosen as the most stable housekeeping gene.

2.13 | Western blot analysis

Frozen skin samples collected on Days 0, 3, 5, and 21 after injury were powdered in liquid nitrogen using a prechilled mortar and pestle and then homogenized in RIPA buffer containing protease inhibitor cocktail (Sigma-Aldrich Co.), phosphatase inhibitor cocktail (Sigma-Aldrich Co.), and phenylmethanesulfonyl fluoride (PMSF, Sigma-Aldrich Co.), followed by sonication (3×5 s) with a sonicator (Vibra-Cell VCX 130 PB). Total cell lysates (keratinocytes) were prepared in 100–400 μl RIPA buffer containing protease inhibitor cocktail (Sigma-Aldrich Co.), phosphatase inhibitor cocktail (Sigma-Aldrich Co.), and phenylmethanesulfonyl fluoride (PMSF, Sigma-Aldrich Co.). Protein concentration was measured by the infrared (IR)-based protein quantitation method with a Direct Detect Infrared Spectrometer (Merck). Forty micrograms of protein were separated on 9% Tricine gels and transferred to polyvinylidene difluoride membranes (Merck Millipore). The membranes were incubated separately with anti-keratin 10 (1:2000, Cat# 76318, Abcam), anti-keratin 14 (1:5000, Cat# ab181595, Abcam), anti–VE-cadherin (1:500, Cat# 331680, Abcam), anti-CCN2 (1:1500, Cat# PA5105312, Invitrogen**),** and anti-β-actin (1:1000, Cat# 8226, Abcam), followed by incubation with fluorescent secondary antibodies against IRDye 800 (1:10 000, Cat# 611–132-122, Rockland Immunochemicals, Inc.) or Cy5.5 (1:10 000, Cat# 610–113-121, Rockland Immunochemicals, Inc., PA, USA) or Alexa Fluor 594 (1:1000, Cat#A11037, Invitrogen) for 1 h. Bands were visualized using the ChemiDoc Touch

Imaging System (Bio-Rad Laboratories, Inc.) and analyzed using Image Lab Software (Bio-Rad Laboratories, Inc.) according to the manufacturer's protocol.

2.14 | Histology

Formalin-fixed skin samples were processed, embedded in paraffin, and sectioned at 3 μm. Immunohistochemical staining for the presence of CCN2 (CTGF) (1:200, Cat# ab6992, Abcam) was performed on consecutive skin sections. Antibody binding was detected with the ABC complex (Vectastain ABC kit, Vector Laboratories, Inc.). In the control sections, primary antibodies were substituted with nonspecific immunoglobulin G (IgG). Peroxidase activity was revealed using 3,3′-diaminobenzidine (Sigma-Aldrich Co.) as a substrate. The slides were counterstained with hematoxylin (Sigma-Aldrich Co.). The sections were visualized using an Olympus microscope (BX43), photographed with an Olympus digital camera (XC50), and analyzed with Olympus CellSens Software.

Immunofluorescence detection and colocalization of Foxn1 and Ccn2 were performed on skin samples collected from young Foxn1::Egfp transgenic mice at day 5 post-wounding. For the immunodetection assay, we used skin tissues collected from our previously performed experiment.[56] The samples were fixed in 4% PFA for 2 h, washed in 0.1 M PB (Sigma-Aldrich Co.) overnight at 4 °C, and stored in 18% sucrose (Chempur, Poland)/0.1 M PB solution prior to cryosectioning. Immunofluorescence assays were performed with the following primary antibodies: anti-CCN2 (1:200, Cat# ab96992, Abcam) and anti-eGFP (1:400, Cat# 6673, Abcam). Alexa Fluor 594 (1:200, Cat# A11037, Invitrogen) and Alexa Fluor 488 (1:200, Cat# A 21206, Invitrogen) secondary antibodies were used. Nuclei were counterstained with ProLong Gold Antifade Mountant with DAPI (Invitrogen). Confocal images were scanned and digitalized using an F10i Laser Scanning Microscope integrated with Fluoview Software (Olympus) with a 10×, 60× objective lens. The sequential scans were acquired with Z spacing of 0.5 μm and 512×512 pixel size at room temperature.

2.15 | Statistical methods

A linear mixed-effects model (LMM) was chosen for the analysis. To perform pairwise comparisons among all groups, we estimated marginal means (least squares means) with Tukey's adjustment for multiple comparisons in each case. In the case of experiments that involve repeated measurements on the same strictly defined days/hours for individual groups of the medium, a (linear)

mixed-effects model (LMM) was chosen for the analysis. The significance level was set to 0.05. All calculations were performed in R (version 4.0.2). Estimated marginal means (adjusted for multiple testing in any model) were calculated using the ls means package (version 2.25).

Statistical analysis of *Foxn1* (Figure 1A), *Txn1* (Figure 4B), *Txnrd1* (Figure 4C), *Txn2* (Figure 4D), *Txnrd2* (Figure 4E), *Txnrd3* (Figure 4F), *Ep300* (Figure 5B), and *Vegfa* (Figure 8B) mRNA expression in keratinocytes, keratinocyte migration (Figure 7B), and endothelial cell tube formation (Figure 8D′–F′) was performed with GraphPad Prism, Version 9.0 (GraphPad Software, La Jolla, CA, USA). The data were assessed for normality using the Shapiro–Wilk test. One-way or Two-way analysis of variance (ANOVA) was used. Data are expressed as the mean ± standard deviation (SD). A value of $p < .05$ was considered statistically significant.

3 | RESULTS

3.1 | Proteomic profile of keratinocytes and keratinocyte conditioned media exposed to hypoxic (1% O_2) or normoxic (21% O_2) conditions
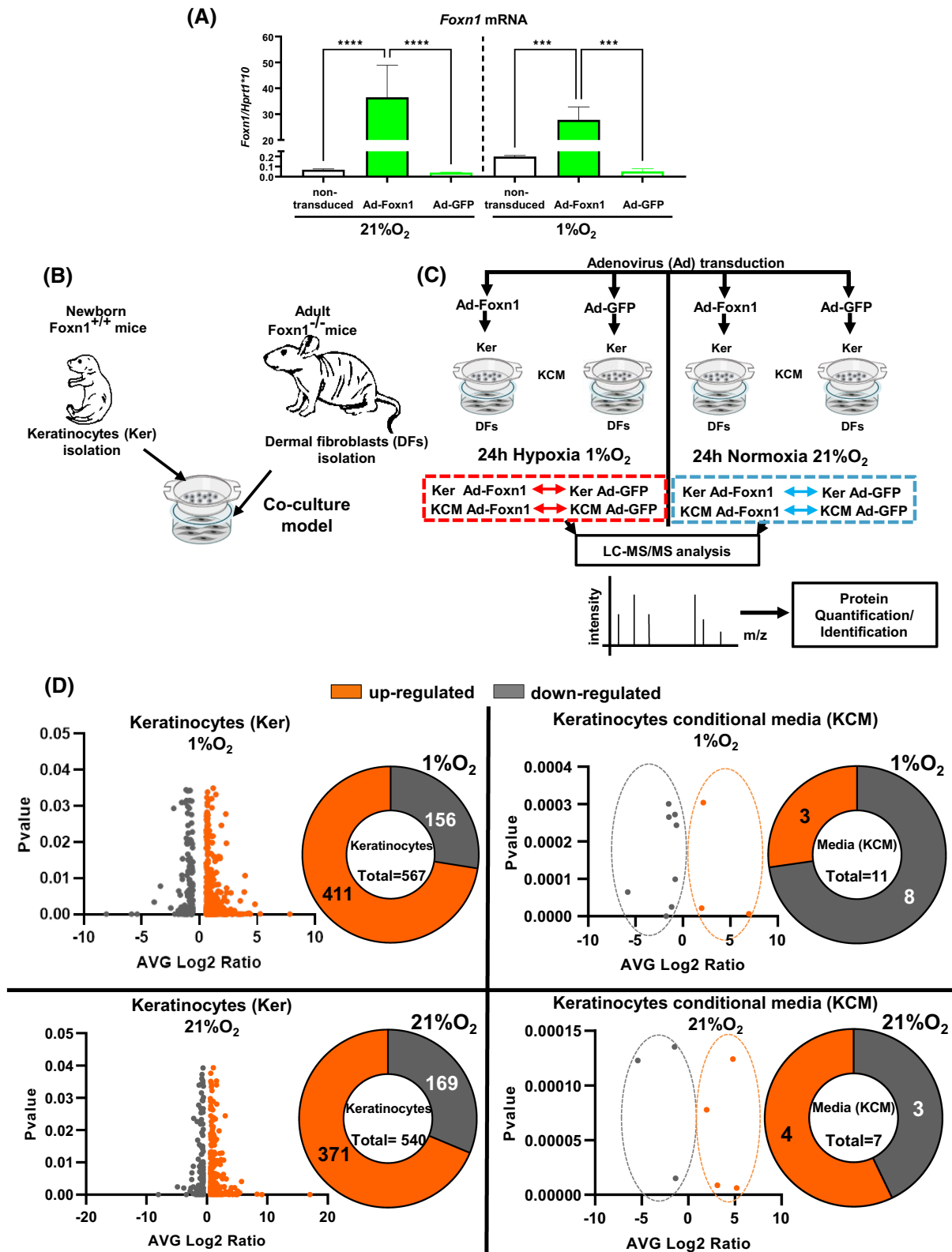
To choose the most appropriate and physiologically relevant model to examine a possible mechanism by which Foxn1 and/or hypoxia regulate physiological changes in keratinocytes, we performed a preliminary experiment (Figure 1A, Figure S1). Primary culture of keratinocytes isolated from Foxn1$^{+/+}$ mice was transduced with Ad-Foxn1 or Ad-GFP and cultured for 24 h under hypoxic (1% O_2) or normoxic (21% O_2) conditions. Followed qRT-PCR analysis showed very high levels of *Foxn1* mRNA expression in Ad-Foxn1-transduced keratinocytes and low in Ad-GFP or non-transduced keratinocytes (Figure 1A). Since in the epidermis, Foxn1 is localized to the suprabasal layer of keratinocytes where it stimulates the first steps of keratinocytes differentiation, we also estimated the levels of keratin 10 (marker of suprabasal keratinocytes) and

keratin 14 (marker of basal keratinocytes) in cultured keratinocytes. The increase in keratin 10 mRNA and protein levels was detected exclusively in Ad-Foxn1-transduced keratinocytes (Figure S1) indicating Foxn1 activity. These data support our previous results that Ad-Foxn1 transduction increases the percent of keratin 10 positive and keratin14/keratin10 double-positive keratinocytes.[57] Based on the presented effectiveness of Ad-Foxn1 transduction, the primary cultures of mouse keratinocytes transduced with Ad-Foxn1 or Ad-GFP (control) were co-cultured with mouse dermal fibroblasts (DFs) under hypoxia (1% O_2) or normoxia (21% O_2) for 24 h (Figure 1B). Afterward, a detailed proteomic analysis of keratinocytes and keratinocyte conditioned medium (KCM) was performed to detect differentially expressed proteins (Figure 1C). In total, ≈5200 proteins were identified from keratinocytes grown under normoxic conditions, and 5000 proteins were identified from cells grown under hypoxia when six replicates were used. When KCM was collected under normoxic growth conditions, approximately 2025 proteins were identified compared to 2100 proteins from hypoxic conditions. The mass spectrometry data have been deposited to Proteomics Identifications Database (PRIDE) with the dataset identifier PXD031125.

LC–MS/MS data were searched against the *Mus musculus* database (SwissProt [5.12.2019]). The quantification values were filtered by a *q*-value (multiple testing corrected *p*-value) of .05 and an absolute log2 ratio of 0.58 by default (see Materials and Methods). The final data are presented as a set of keratinocyte or KCM proteins with differentially up- or downregulated expression after Ad-Foxn1 transduction, separately under hypoxic or normoxic conditions (Figure 1D; Appendix 1–4). Upon Foxn1 stimulation in keratinocytes, a total of 567 proteins under hypoxia and 540 under normoxic conditions were changed (Figure 1D; Appendix 1 and 2). Among the Ad-Foxn1 and hypoxia-stimulated proteins, 411 were increased, whereas 156 showed a decrease. Under normoxic conditions, Foxn1 stimulated 371 proteins and decreased 169 proteins (Figure 1D; Appendix 1 and 2). Similarly, the quantities of more proteins were changed in KCM collected

FIGURE 1 The effectiveness of keratinocytes transduction (A), scheme of proteomics experiment (B,C) and volcano plots/pie chart showing the number of differentially expressed proteins detected in keratinocytes by LC–MS/MS analysis (D). (A) *Foxn1* mRNA expression in keratinocytes collected from the Foxn1$^{+/+}$ (C57BL/6J) mice that were non-transduced or transduced with Ad Foxn1 or Ad-GFP and cultured for 24 h under normoxic (21% O_2) or hypoxic (1% O_2) conditions. (B,C) Keratinocytes collected from the Foxn1$^{+/+}$ (C57BL/6J) mice were transduced with Ad Foxn1 or Ad-GFP and co-cultured for 24 h with DFs collected from the Foxn1$^{-/-}$ (CBy. Cg-Foxn1 <nu>/ cmdb) mice under normoxic or hypoxic conditions ($n = 3$, 2 animals per experiment, total $n = 6$ animals). Keratinocyte and keratinocyte conditional media (KCM) were subjected to detailed mass spectrometry analysis. (D) Total number of differentially regulated proteins in keratinocytes or KCMs upon Ad-Foxn1 transduction cultured under hypoxic or normoxic conditions (donut graph). Corresponding volcano plots illustrate the AVG log2 ratio (i.e., fold changes expressed as log2 transformed ratios of averaged replicates). The *p*-value was calculated as the inverse cumulative distribution function of the decoy distribution for a given discriminant score (Spectronaut Cscore). Data were filtered with a *q*-value below or equal to .05 and an absolute log2 ratio equal to or above 0.58 by default.

(A) *Foxn1* mRNA

(B) Newborn Foxn1^{+/+} mice — Keratinocytes (Ker) isolation; Adult Foxn1^{-/-} mice — Dermal fibroblasts (DFs) isolation; Co-culture model

(C) Adenovirus (Ad) transduction

(D) up-regulated / down-regulated

from the Ad-Foxn1-transduced keratinocytes cultured under hypoxic[11] than normoxic[7] conditions (Figure 1D; Appendix 3 and 4). However, upon Ad-Foxn1 stimulation, 8 out of 11 proteins decreased under hypoxic conditions, whereas only 3 out of 7 decreased under normoxic conditions (Figure 1D).

To determine whether the protein profiles reveal intrinsic biological differences upon Ad-Foxn1 stimulation in normoxia or hypoxia, we performed Gene Ontology (GO) enrichment analysis with differentially expressed proteins detected in keratinocytes (Figure 2A,B, Figure S2) or KCM (Figure S3). Genes

(A)
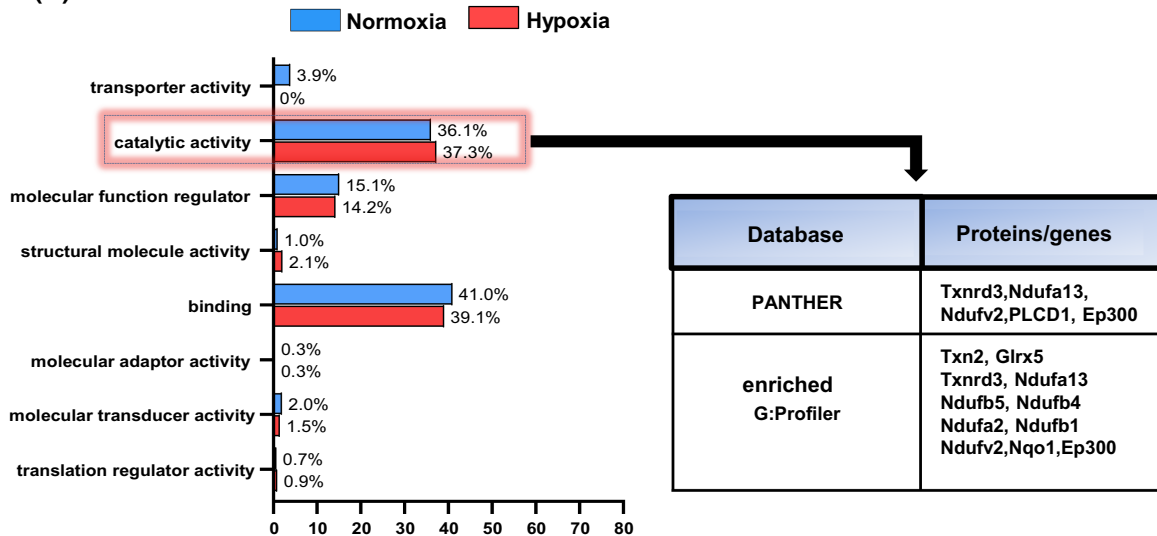
(B)
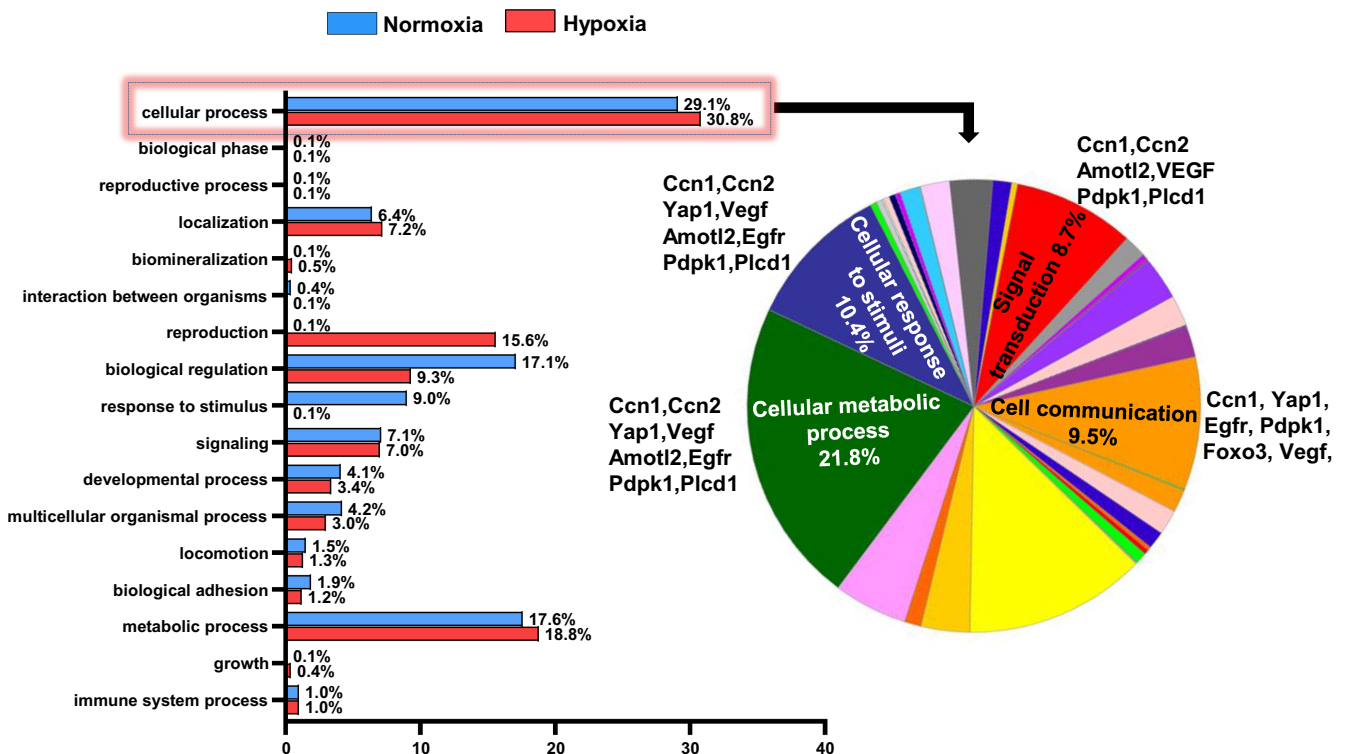
FIGURE 2 Classification of proteins regulated upon Foxn1 transduction into keratinocytes and exposed for 24 h to hypoxia (1% O2) or normoxia (21% O2) according to Gene Ontology (GO) classification using PANTHER and enriched with g: Profiler database. Diagrams illustrate detected proteins in terms of (A) molecular function (with detailed proteins included in the catalytic activity class), and (B) biological processes (with the proteins included in the cellular processes class). Table (A) and pie chart (B) correspond to the category of highlighted proteins.

were classified into four main GO categories: molecular function (Figure 2A), biological processes (Figure 2B), cellular component (Figure S2A), and protein class

(Figure S2B) using the PANTHER Classification System, which was enriched with analysis by the g:Profiler database (Figure 2A). The distribution of proteins with

up- and downregulated expression upon Foxn1 transduction is presented in Figure S4A–H.

Within the molecular function category, overexpression of Foxn1 in keratinocytes led to changes in the proteins included in the catalytic activity (36.1% Nor. vs. 37.3% Hyp.), binding class (41% Nor. vs. 39.1% Hyp.), and molecular function regulator groups (15.1% Nor. vs. 14.2% Hyp.; Figure 2A). These proteins showed comparable distributions under normoxic and hypoxic conditions (Figure 2A) and similar directions of regulation (Figure S4E,F). Within the catalytic activity, redox proteins (systems of Txn and GSH) constitute a significant part of this protein class (Figure 2A). In KCM, proteins in molecular function categories were involved in catalytic activity (40% Nor. vs. 60% Hyp.), act as molecular function regulators but exclusively under normoxic conditions (20% Nor. vs. 0% Hyp.), and belong to the binding class, regardless of hypoxia or normoxia (40% Nor. vs. 40% Hyp.) (Figure S3C).

The biological process category encompassed proteins associated with cellular (29.1% Nor. vs. 30.8% Hyp.), metabolic processes (17.6% Nor. vs. 18.8% Hyp.), and biological regulation (17.1% Nor. vs. 9.3% Hyp.) that were predominantly regulated upon Foxn1 stimulation (Figure 2B). Detailed analysis of the cellular processes category revealed a group of proteins, including Ccn1, Ccn2, Yap1, Vegfa, Amotl2, Egfr, Pdpk1, and Plcd1, that are involved in cell communication, signal transduction, response to stimuli, and metabolic processes, among others (Figure 2B). Proteins secreted into KCM upon Foxn1 overexpression in keratinocytes within the categories of biological processes showed the highest involvement in cellular processes (21.4% Nor. vs. 26.1% Hyp.), biological regulation (21.4% Nor. vs. 8.7% Hyp.), metabolic process (14.3% Nor. vs. 13% Hyp.), and response to stimulus (21.4% Nor. vs. 17.4% Hyp.) (Figure S3D).

Data related to the functionality of proteins were obtained from the Gene Ontology analysis (PANTHER, enriched with g:Profiler; Figure 2A) and from the Kyoto Encyclopedia of Genes and Genomes (KEGG) pathway analysis (Figure S5) prompted us to further investigate their possible interactions that could affect skin homeostasis. For this purpose, we investigated the interactions between Foxn1-enriched proteins using network models deposited in the STRING database (http://string-db.org). Strong protein correlations defined by the database combined with our previous in vitro and in vivo data[40,41] allowed us to extract a map of the protein network. The interactive map visualizes a coherent network of cascading activation of cellular processes that are involved in the control of skin function, including skin wound healing (Figure 3A,B). These proteins were divided into two interacting clusters (Figure 3A). The first group was defined as an oxidoreductase cluster that contains Foxn1-stimulated proteins involved in electron transport (Ndufa13, Ndufb5, Ndufb4, Ndufa2, Ndufb1, Ndufv2, Romo1) and an oxidoreductase system: thioredoxin-glutathione (Txn1, Txnrd1, Txn2, Txnrd2 Glrx5, Txnrd3, Srxn1), identified mostly under hypoxic conditions, which is characteristic of the first steps of the skin wound healing process. Undoubtedly, the reduced oxygen availability activated hypoxia-induced proteins (Ep300, Hif-1α), which, along with the oxidoreductase system, acted on the second group of proteins, defined as functional clusters (Figure 3A). The functional cluster contains proteins involved in migration/proliferation (Ccn1, Ccn2, Yap1), signaling (Egfr, Pdpk1, Plcd1), and angiogenesis (Vegf, Timp3, Amotyl2) (Figure 3B). Intriguingly, most of these proteins had downregulated expression after Foxn1 stimulation (compared with Ad-GFP) under both normoxic and hypoxic conditions.

3.2 | Foxn1 regulates the thioredoxin system

Changes in Txn1, the cytoplasmic form of Txns, upon Foxn1 action were detected in our previous study.[45,57] The transcriptomics data[21] were confirmed by protein analysis showing low levels of Txn1 in the epidermis of uninjured and injured Foxn1$^{-/-}$ skin.[45] Current LC–MS/MS analysis of proteins extracted from the Ad-Foxn1-transduced keratinocytes revealed the regulation of proteins that belong to the oxidoreductase cluster, including those of the Txn system (Txn2 and Txnrd3) (Figure 4A). To confirm and validate the proteomic data, we performed RT-qPCR on independent biological samples (Figure 4B–F). Verification was performed on keratinocytes isolated from the Foxn1$^{+/+}$ mice (Keratinocytes Foxn1$^{+/+}$) that were transduced with Ad-Foxn1 or Ad-GFP or non-transduced, and keratinocytes isolated from the Foxn1$^{-/-}$ mice (Keratinocytes Foxn1$^{-/-}$) transduced with Ad-Foxn1 or Ad-GFP (Figure 4B–F). Keratinocytes were cultured under hypoxic or normoxic conditions for 24h (Figure 4B–F). To confirm the results at the in vivo (systemic model) level, we also analyzed uninjured and injured skin collected from the Foxn1$^{-/-}$ and Foxn1$^{+/+}$ mice (Figure 4G–J, Tables S1–S5).

Cytoplasmic *Txn1* (Figure 4B) and *Txnrd1* (Figure 4C) mRNA expression levels analyzed in cultured keratinocytes showed no differences regardless of transduction (Ad-Foxn1 vs Ad-GFP) or culture conditions (1% O_2 vs 21% O_2) in both keratinocytes isolated from Foxn1$^{+/+}$ or Foxn1$^{-/-}$ mice. The total skin samples examination of intact (Day 0) and post-injured tissues (Days 1–21) showed low levels of *Txnrd1* mRNA expression in Foxn1$^{-/-}$ mice
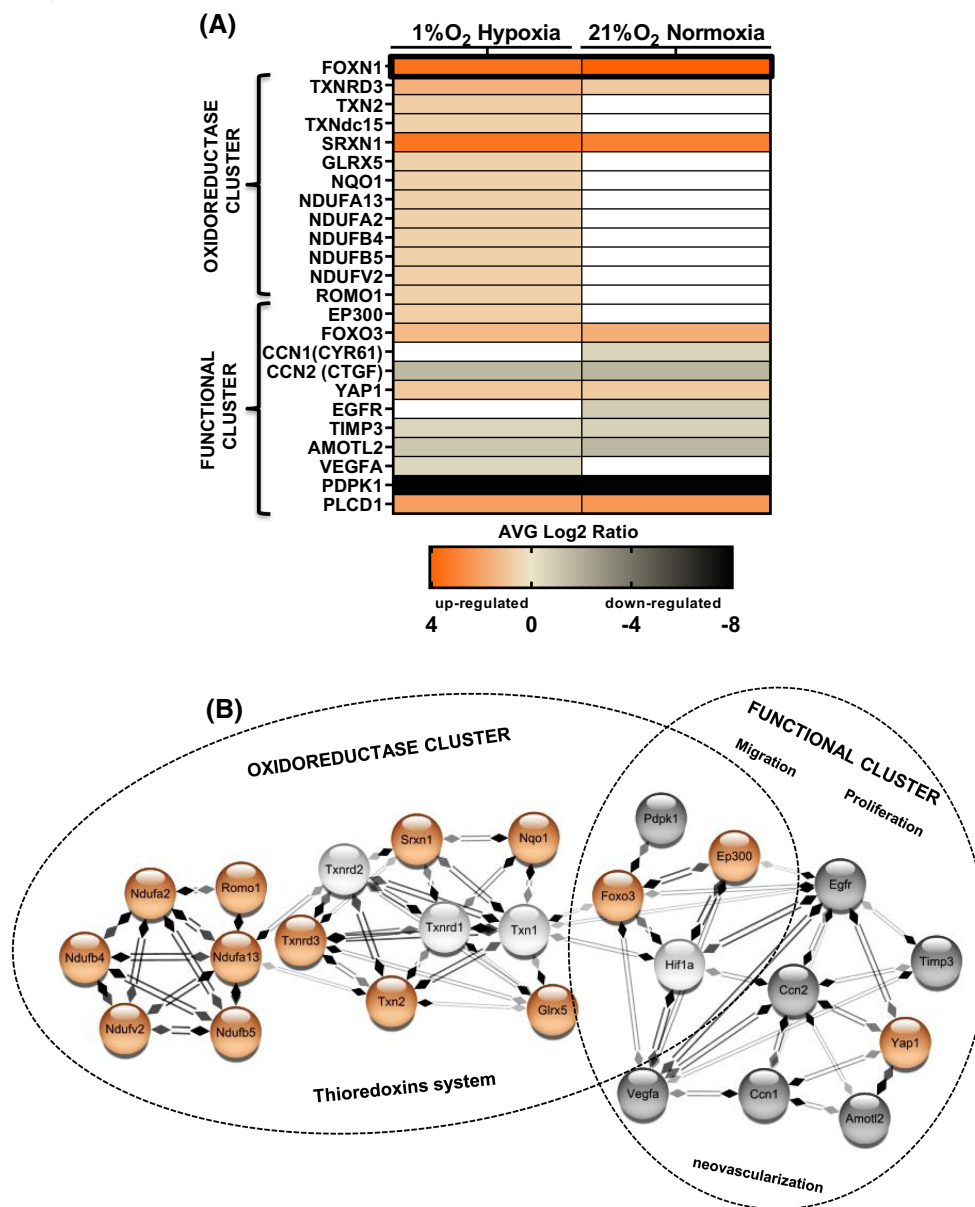
FIGURE 3 Heatmap (A) and protein–protein interaction networks (B) of differentially expressed Foxn1 action-regulated proteins following hypoxic or normoxic conditions were selected on the basis of Gene Ontology (GO) and analyzed in the STRING online database, version 11.0. (A) Heatmap shows Foxn1-enriched proteins selected on the basis of Gene Ontology analysis (PANTHER, enriched with g:Profiler). The scale bar in the heatmap indicates protein fold changes ranging from +4 to −8. (B) Interactions among Foxn1-regulated proteins using network map models deposited in the STRING database. The lines indicate the strength of data on medium score >0.4. Interactions of the proteins with upregulated (orange spheres) or downregulated (gray spheres) expression upon hypoxia. Proteins marked as white spheres were identified in our previous analyses (e.g., Txn1, Hif-1α) or were strongly correlated to detected proteins by the database (e.g., Txnrd1, Txnrd2).

on post-injured days 3–21 (Figure 4G, Table S1), consistent with the low levels of Txn1 protein previously identified in Foxn1$^{-/-}$ mice skin.[45]

Txn2, the mitochondrial form of Txn, displayed no differences in mRNA levels related to adenoviral transduction or culture conditions for Foxn1$^{+/+}$ and Foxn1$^{-/-}$ keratinocytes (Figure 4D). The analysis of *Txn2* expression in the skin showed slightly higher mRNA levels in the Foxn1$^{-/-}$ injured skin (Days 5, 7, and 21), although the

data did not reach statistical significance (Figure 4H). *Txnrd2* displayed the highest levels of mRNA expression in non-transduced Foxn1$^{+/+}$ keratinocytes cultured under hypoxic conditions (Figure 4E). Interestingly, adenoviral transduction, regardless of Ad-Foxn1 or Ad-GFP, reduced levels of *Txnrd2* mRNA expression (Figure 4E). Skin samples from the Foxn1$^{+/+}$ and Foxn1$^{-/-}$ mice showed similar and generally stable levels of *Txnrd2* expression, although on post-wounding Day 1, high levels of
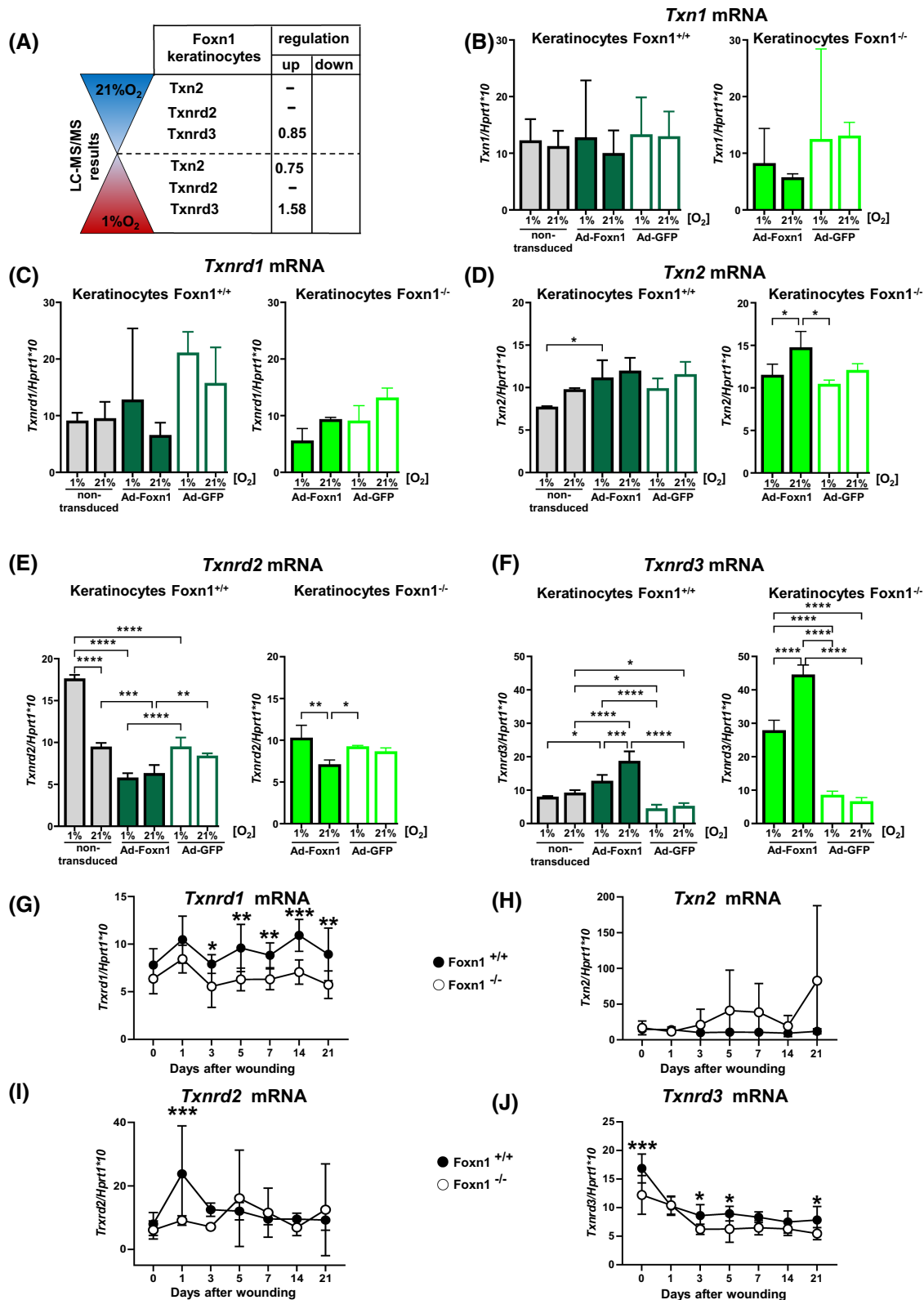
FIGURE 4 Foxn1 modulates antioxidant defense in keratinocytes (A-F) and during skin wound healing (G-J). Keratinocytes isolated from the Foxn1$^{+/+}$ or Foxn1$^{-/-}$ mice were co-cultured with DFs for 24h under hypoxic (1% O$_2$) or normoxic (21% O$_2$) conditions. Prior to co-culture, keratinocytes from the Foxn1$^{-/-}$ mice were transduced with Ad-Foxn1 or Ad-GFP (control). (A) Differences in Txn2, Txnrd2, and Txnrd3 protein levels (LC–MS/MS) in keratinocytes upon Foxn1 transduction and culture: hypoxia vs. normoxic conditions. (B) *Txn1*, (C) *Txnrd1*, (D) *Txn2*, (E) *Txnrd2*, and (F) *Txnrd3* mRNA expression in cultured keratinocytes ($n = 3$–4). (G) *Txnrd1*, (H) *Txn2*, (I) *Txnrd2*, and (J) *Txnrd3* mRNA expression in uninjured (Day 0) and injured (Days 1–21) skin of the Foxn1$^{+/+}$ and Foxn1$^{-/-}$ mice ($n = 6$ samples per day per group). Values are the lsmean±SE; asterisks indicate significant differences between normoxic versus hypoxic culture conditions (B–F), Ad-Foxn1 versus Ad-GFP transduced keratinocytes (B–F), or between Foxn1$^{-/-}$ and Foxn1$^{+/+}$ mice (G–J) during the skin wound healing process (*$p < .05$; **$p < .01$; ***$p < .001$).

(A)

(B)   *Ep300* mRNA

(C)
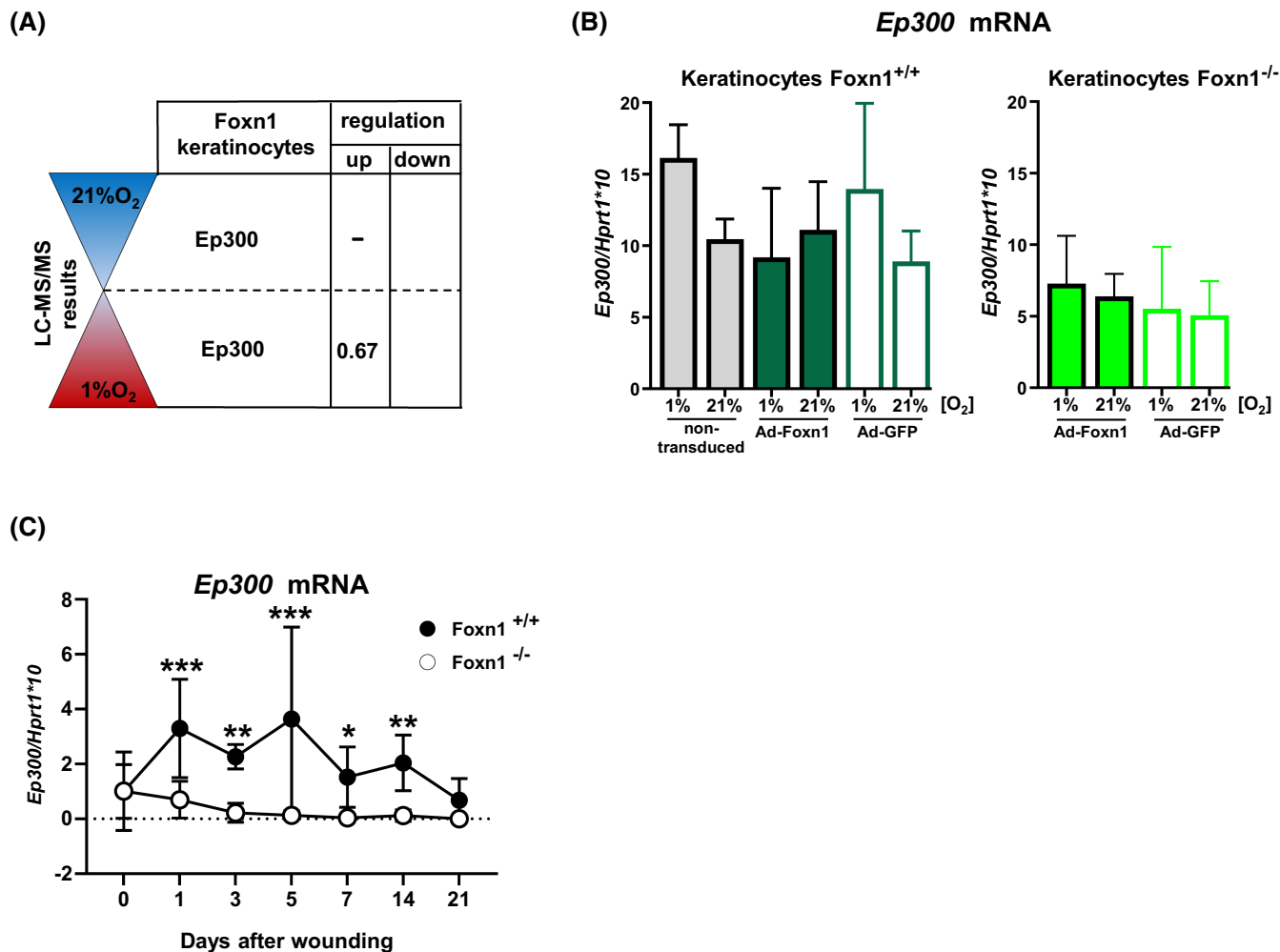
FIGURE 5 Ep300 protein levels (A) and mRNA (B-C) expression are modulated in keratinocytes (B) and in wounded skin (C). (A) Differences in Ep300 protein levels (LC–MS/MS) in keratinocytes upon Foxn1 transduction and culture conditions: hypoxia versus normoxia. (B) qRT-PCR analysis of *Ep300* mRNA expression in keratinocytes (C) qRT-PCR analysis of Ep300 mRNA expression in uninjured (Day 0) and injured (Days 1–21) skin. Values are the lsmean ± SE; asterisks indicate significant differences between normoxic or hypoxic culture conditions (B), Ad-Foxn1 versus Ad-GFP-transduced keratinocytes (B), or between Foxn1$^{-/-}$ and Foxn1$^{+/+}$ mice (C) during the skin wound healing process (*$p < .05$; **$p < .01$; ***$p < .001$).

expression were detected in the Foxn1$^{+/+}$ mice (Figure 4I, Tables S2 and S3).

Intriguingly, the most appealing results were obtained for *Txnrd3* mRNA expression, in which protein levels in proteomics analysis were increased upon Foxn1 stimulation, particularly under hypoxic conditions (Figure 4A). Ad-Foxn1 transduction regardless of keratinocytes origin (Foxn1$^{+/+}$ or Foxn1$^{-/-}$ mice) caused a robust surge of *Txnrd3* mRNA expression levels (Figure 4F). The increase in *Txnrd3* mRNA was significantly higher under normoxic conditions in Ad-Foxn1 transduced keratinocytes (Figure 4F). Moreover, the in vivo data confirmed higher levels of *Txnrd3* mRNA in the skin of the Foxn1$^{+/+}$ mice in both uninjured (Day 0; $p < .001$) and injured tissues (Days 3, 5, 21) (Figure 4J, Tables S4 and S5).

Thus, current in vitro and in vivo results together with our previous data[45] indicated a strong contribution of

Foxn1 to antioxidant defense in keratinocytes by acting on the Txn system.

3.3 | Ep300, the Hif-1α coactivator, shows upregulated expression upon skin injury in the Foxn1$^{+/+}$ mice

Our previous in vivo study revealed that the skin of the Foxn1$^{-/-}$ compared to Foxn1$^{+/+}$ mice responds to wounding with a significant decrease in Hif-1α content analyzed at both the mRNA and protein levels. In contrast, the expression of Fih-1 (a Hif-1α inhibitor) was elevated in the wounded skin of the Foxn1$^{-/-}$ versus Foxn1$^{+/+}$ mice.[45] The present proteomic data indicated that Ep300 (Hif-1α coactivator) is a factor that is stimulated by Foxn1 under hypoxic conditions (Figure 5A).

However, Ad-Foxn1 transduction into the Foxn1$^{-/-}$ or Foxn1$^{+/+}$ keratinocytes did not stimulate *Ep300* mRNA expression (Figure 5B). Likewise, in an in vivo setting, *Ep300* mRNA levels were similar between the Foxn1$^{+/+}$ and Foxn1$^{-/-}$ mice in uninjured skin; however, the expression was changed diametrically upon injury. On post-wounding day 1, upregulation of *Ep300* mRNA levels was observed exclusively in the Foxn1$^{+/+}$ mice ($p < .001$; Figure 5C) and was sustained until post-wounding day 14 (Figure 5C; Tables S6 and S7).

3.4 | Foxn1 decreases connective tissue growth factor 2 (Ccn2) activity

Detailed mass spectrometry analysis of proteins isolated from keratinocytes and KCM upon Foxn1 stimulation identified a group of proteins that belong to the CCN family (Figure 2B; Appendix 1–4). The data showed that Foxn1 stimulation downregulated Ccn1 and Ccn2 levels in keratinocytes and Ccn2 in KCM regardless of oxygen availability (hypoxic or normoxic conditions) (Figure 6A). Consequently, we investigated the above results in an in vivo model and evaluated Ccn2 protein levels in the skin of the Foxn1$^{+/+}$ and Foxn1$^{-/-}$ mice during wound healing (Figure 6B). Western blot analysis showed that wounded skin samples collected from the Foxn1$^{+/+}$ mice contained lower levels of Ccn2 protein than those of the Foxn1$^{-/-}$ mice on Days 3, 5, and 21 (Figure 6B). The data are in agreement with the proteomic results indicating that the presence of Foxn1 (Ad-Foxn1 in keratinocyte culture or in the skin of the Foxn1$^{+/+}$ mice) downregulates Ccn2 protein levels (Figure 6A,B). To estimate Ccn2 skin localization, we performed immunohistochemical staining for Ccn2 in the skin of the Foxn1$^{+/+}$ and Foxn1$^{-/-}$ mice (Figure 6C). Ccn2 protein was detected in uninjured epidermis and hair follicles, and its presence became much stronger in injured skin, particularly in the neoepidermis. However, the reactivity was much stronger in the Foxn1$^{-/-}$ mice (Figure 6C).

Since both Foxn1 and Ccn2 are known to be expressed in epithelial cells of the epidermis and in hair follicles, we performed colocalization analysis (Figure 6D). Using wounded skin samples from transgenic Foxn1::Egfp mice, in which an enhanced green fluorescent protein transgene is driven by Foxn1 regulatory sequences,[56] we performed double fluorescent staining for Foxn1 and Ccn2 (Figure 6D). Confocal imaging presented strong colocalization of eGFP (Foxn1) and Ccn2 in the epidermis adjacent to the wounded area and at the wound margin that was confined to the suprabasal but not the basal layer of the epidermis (Figure 6D).
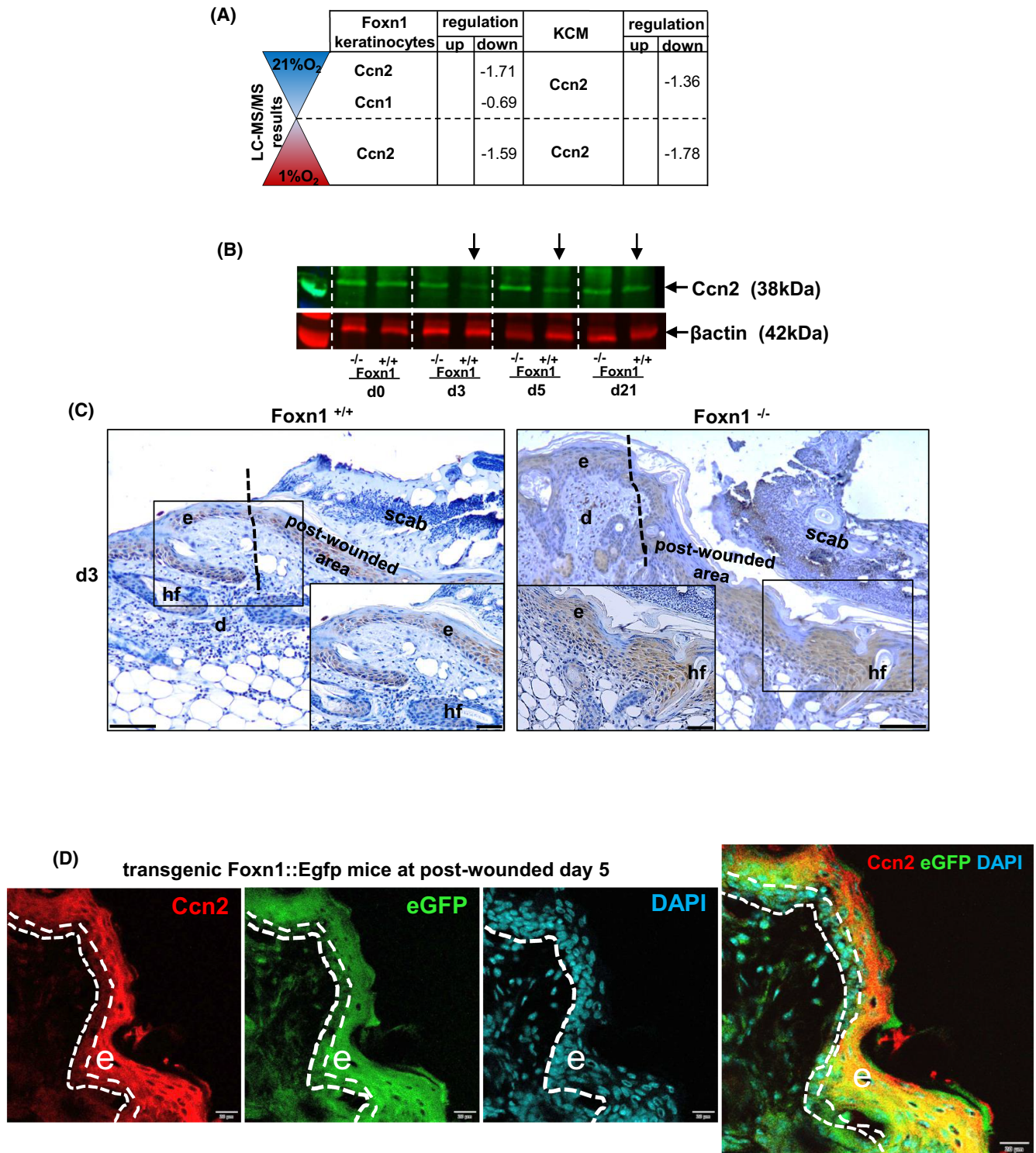
3.5 | Foxn1 and hypoxia regulate the physiological/functional changes of keratinocytes

As multifunctional matricellular proteins, CCNs are involved in several processes, including cell proliferation, migration, angiogenesis, and interactions with connective tissue.[7] A combination of the proteomic in vitro results together with the results related to Ccn2 protein expression in vivo led to a functional cluster (see Figure 3) analysis to assess the proliferative and migratory abilities of keratinocytes stimulated by Foxn1 under hypoxic or normoxic conditions and the neovasculatory abilities of related KCMs (Figures 7 and 8).

For this purpose, keratinocytes transduced with Ad-Foxn1 or Ad-GFP (control) were cultured for 24 h under hypoxic (1% O_2) or normoxic (21% O_2) conditions. To assess the keratinocyte migratory index upon Foxn1 and/or oxygen availability, we performed an in vitro wound (scratch) assay (Figure 7A–D, Tables S8–S11). Low oxygen content (hypoxia), as a single variable, accelerated keratinocyte migration, particularly at 3 and 6 h after scratching (Figure 7A,B, Tables S8). However, Foxn1 had the most profound effect on keratinocyte migration (Figure 7A,C,D, Tables S8–S11). Moreover, this effect was strongly modulated by oxygen environmental conditions (Figure 7A,C,D, Tables S8–S11). Whereas hypoxia stimulated the migration of keratinocytes, Foxn1 overexpression under the same conditions (hypoxia) significantly slowed the process as observed between (3 and 24 h of culture; Figure 7D, Table S9). In contrast, overexpression of Foxn1 in keratinocytes that were cultured under normoxic conditions accelerated migration, particularly at 3 and 6 h of culture (Figure 7C; Table S11).

Next, we analyzed the effect of oxygen availability and Foxn1 overexpression on keratinocyte viability (Figure 7E) and proliferation rate (Figure 7F, Table S12). Hypoxia stimulated both metabolic and proliferation rates regardless of the presence of Foxn1, although statistical significance was obtained exclusively for proliferation ($p < .01$; Figure 7F, Table S12).

Angiogenesis and vascular formation are regulated by Vegfa; the protein that together with Amotl2 showed downregulated expression with Foxn1 in keratinocytes regardless of oxygen conditions (Figure 8A; Appendix 2). To verify the proteomic data, we analyzed *Vegfa* mRNA expression levels (Figure 8B,C), CD31-positive cell localization (Figure S6A), and VE-cadherin (vascular endothelial cell cadherin) protein levels (Figure S6B). The *Vegfa* mRNA expression levels were analyzed in independent biological samples of keratinocytes collected from Foxn1$^{+/+}$ mice: non-transduced or transduced with Ad-Foxn1 or Ad-GFP and those collected from the Foxn1$^{-/-}$ mice that

(A)

LC-MS/MS results	Foxn1 keratinocytes	regulation		KCM	regulation	
		up	down		up	down
21%O₂	Ccn2		-1.71	Ccn2		-1.36
	Ccn1		-0.69			
1%O₂	Ccn2		-1.59	Ccn2		-1.78

(B)

← Ccn2 (38kDa)

← βactin (42kDa)

-/-	+/+	-/-	+/+	-/-	+/+	-/-	+/+
Foxn1		Foxn1		Foxn1		Foxn1	
d0		d3		d5		d21	

(C)

(D)

FIGURE 6 Foxn1 Alters CCN2 protein levels in keratinocytes and the corresponding KCM (A) and in injured skin (B–D). (A) Levels (LC–MS/MS) of CCN1 and CCN2 proteins upon Foxn1 transduction and culture conditions: Hypoxia versus normoxia in keratinocytes or in corresponding KCM. (B) Representative Western blot analysis of Ccn2 and β-actin (reference) proteins in the intact (Day 0) and injured (Days 3, 5, and 21) skin of the Foxn1$^{-/-}$ and Foxn1$^{+/+}$ mice. (C). Immunohistochemical detection of Ccn2 localization in the skin of the Foxn1$^{-/-}$ and Foxn1$^{+/+}$ mice collected at post-wounding day 3. (D) Colocalization of Ccn2 and Foxn1 was performed on skin samples collected from the transgenic Foxn1::Egfp mice at day 3 post-wounding. e-epidermis; d-dermis; hf-hair follicles, dotted line-demarcation of the suprabasal layer from the basal layer. Scale bar (C) 200 μm, (insets; 50 μm); and (D) 200 μm (confocal images; inset 20 μm).
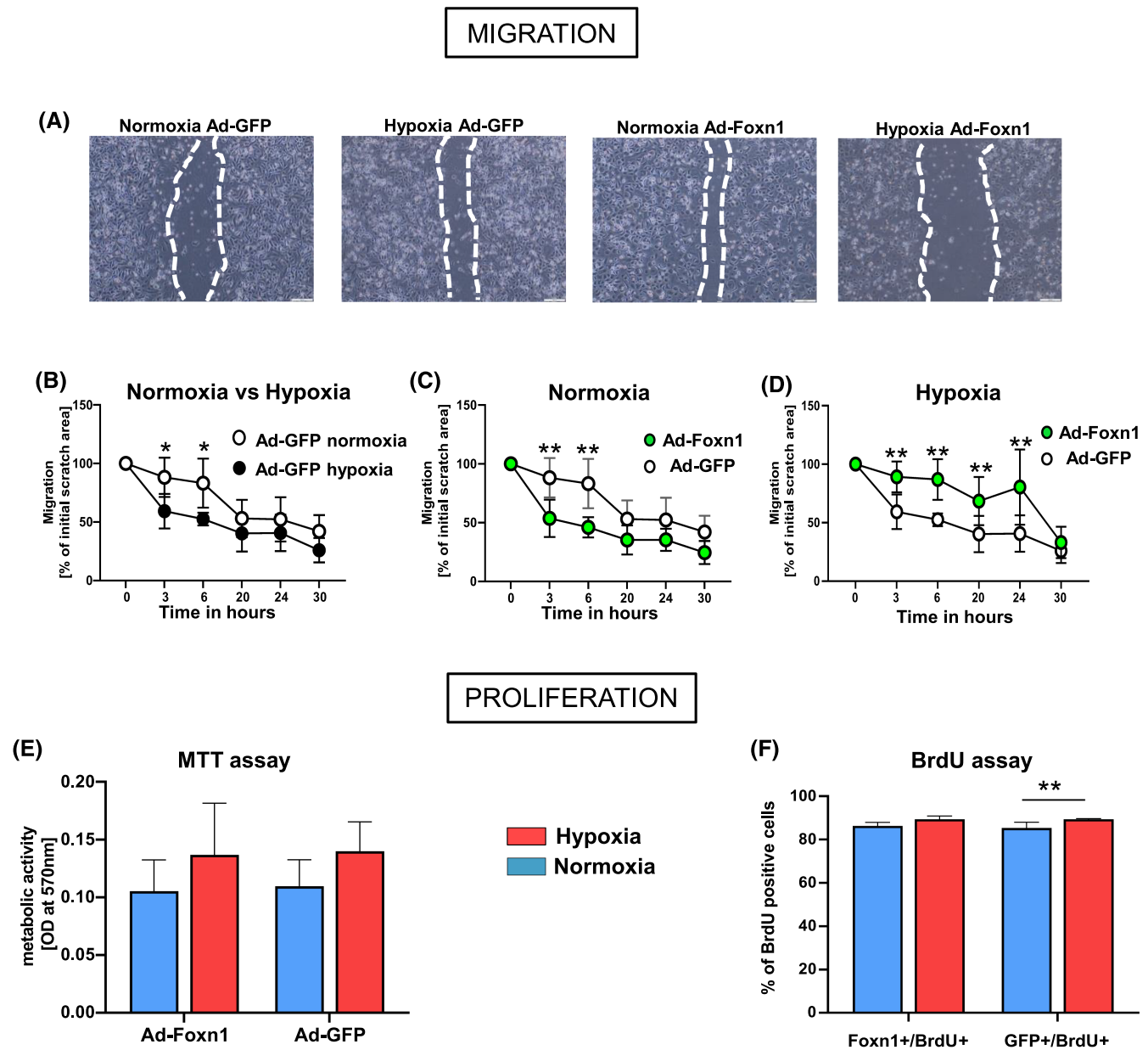
MIGRATION

FIGURE 7 Oxygen availability (normoxia vs. hypoxia) and Foxn1 modulate keratinocyte migration and proliferation. (A) Representative photos of keratinocytes transduced with Ad-Foxn1 or Ad-GFP and wounded keratinocytes (scratch in vitro assay) that were cultured under hypoxic or normoxic conditions. Images were taken at 24 h. (B–D) Analysis of the migratory abilities of keratinocytes transduced with Ad-Foxn1 or Ad-GFP, wounded (scratch assay) and cultured under hypoxic or normoxic conditions ($n = 4$). (E) MTT assay. Absorbance assessing the metabolic activity of keratinocytes transduced with Ad-Foxn1 or Ad-GFP and cultured under hypoxia or normoxia ($n = 5$). (F) BrdU incorporation assay followed by flow cytometric analysis of keratinocytes transduced with Ad-Foxn1 or Ad-GFP and cultured under hypoxia or normoxia showing the percentage of BrdU-incorporating cells ($n = 5$). Values are the lsmean ± SE; asterisks indicate significant differences between normoxic or hypoxic conditions or Foxn1 versus GFP transduction ($*p < .05$; $**p < .01$).

were transduced with Ad-Foxn1 or Ad-GFP (Figure 8B). The upregulation of *Vegfa* mRNA levels was detected exclusively under hypoxic conditions regardless of keratinocytes origin (Foxn1$^{-/-}$ or Foxn1$^{+/+}$ mice) or transduction (Ad-Foxn1 or Ad-GFP). Furthermore, Foxn1 transduced into both: keratinocytes Foxn1$^{+/+}$ and keratinocytes Foxn1$^{-/-}$ decreased levels of *Vegfa* mRNA expression in comparison to Ad-GFP transduced keratinocytes

or non-transduced (Figure 8B) confirming proteomics results (Figure 8A). The *Vegfa* mRNA in vivo expression levels did not significantly differ between the uninjured and injured skin samples collected from Foxn1$^{-/-}$ and Foxn1$^{+/+}$ mice (Figure 8C). However, a decreased accumulation of CD31-positive cells (Figure S6A) and lower levels of VE-cadherin protein (Figure S6B) were detected in uninjured skin samples collected from Foxn1$^{+/+}$ mice.

These in vivo data (Figure S6A,B) support the proteomics results (Figure 8A) indicating lower angiogenic potential at Foxn1 presence.

Next, we examined the possible effect of KCMs collected from keratinocytes transduced with Ad-Foxn1 or Ad-GFP and cultured for 24 h under hypoxia or normoxia on the angiogenic process in vitro. Human umbilical vein endothelial cells (HUVECs) were incubated with different KCMs. The tube formation assay performed at 6, 12, and 18 h of culture revealed the presence of three groups of endothelial

VASCULARIZATION
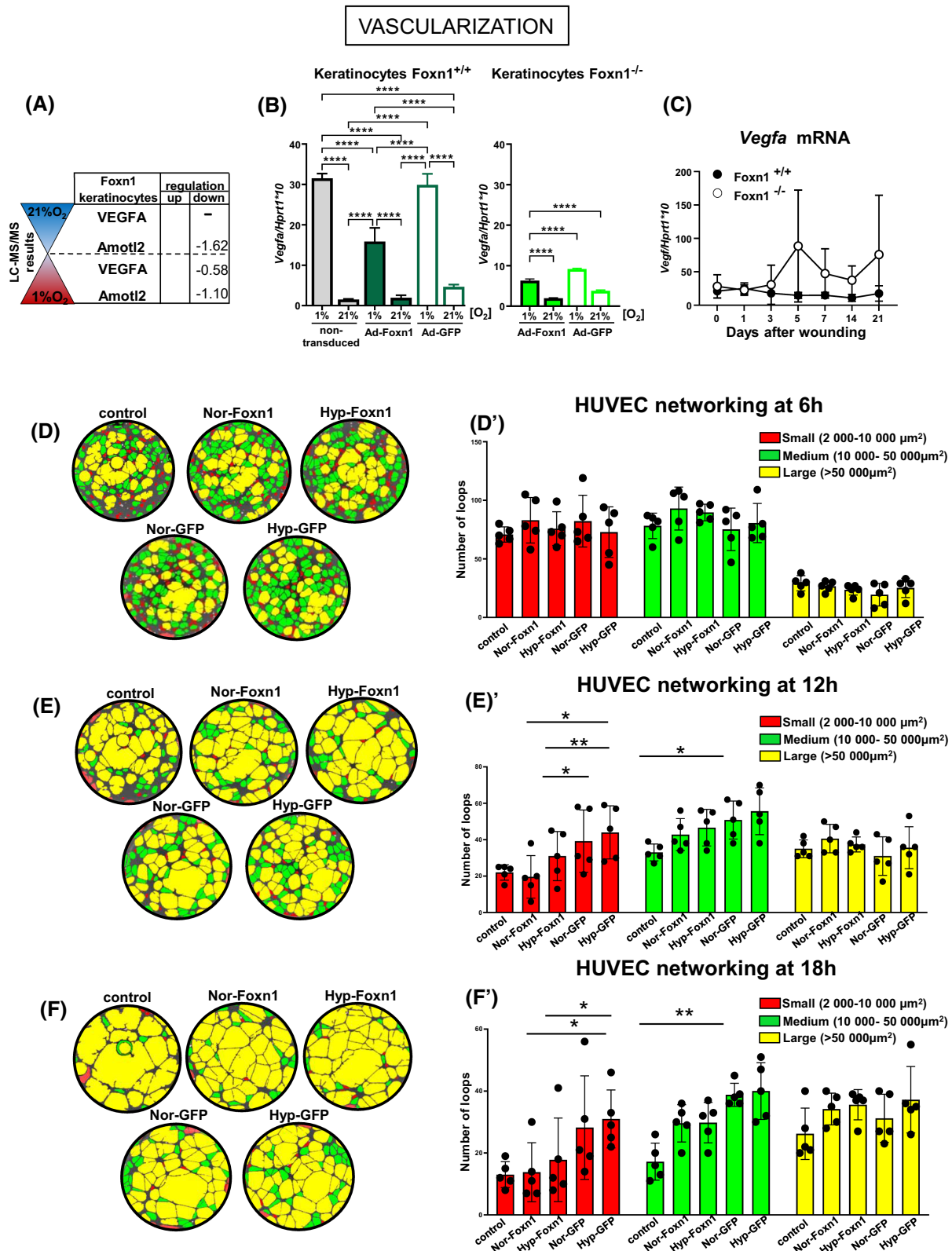
loops separated by size: small (2000–10 000 μm^2), medium (10 000–50 000 μm^2), and large (>50 000 μm^2), regardless of the type of medium (Figure 8D–F,D′–F′). After 6 h of culture, the number of small- and medium-sized tubes represented the most abundant type of endothelial network; however, we did not observe any significant differences in the rate of vascular formation regardless of the applied KCMs (Figure 8D–F). At 12 h, HUVECs cultured in KCM-Hyp-GFP showed an increase in the number of small-sized and medium-sized loops compared to those cultured in KCM-Nor-Foxn1 ($p < .01$; Figure 8E) or to control cultures ($p < .05$; Figure 8E). Subsequently, at a longer time lapse (18 h), KCM-Hyp-GFP continued to maintain a higher number of small- and medium-sized tubes ($p < .05$; Figure 8F). Thus, KCM-Hyp-GFP showed greater proangiogenic activity than KCM-Nor/Hyp-Foxn1 and controlled proangiogenic activity by extending the maintenance of small- and medium-sized cell loops during the experimental time course.

4 | DISCUSSION

The internal (cellular and molecular) and external (environmental) components regulate skin function. Keratinocytes, the major cellular element of the epidermis, act as a first barrier that responds to environmental threads, for example, injury or UV radiation. Triggered by injury, keratinocytes activate transcription factors that regulate downstream effector genes, coordinating not only epidermal reconstruction but also release factors that regulate the dermal repair process.

In the present study, we focused on keratinocytes, the transcription factor Foxn1, and oxygen availability, the components that collectively sustain skin homeostasis and regulate the response to injury. To investigate a possible mechanism by which Foxn1 under hypoxic or normoxic conditions regulates physiological changes in keratinocytes at the molecular and functional levels, we used detailed mass spectrometry analysis (LC–MS/MS), followed by in vitro and in vivo experiments. We demonstrated in vitro and in vivo that Foxn1 regulates[1] the antioxidant

defense system, particularly through the Txn system[2]; the migration of keratinocytes through Ccn2 alteration; and[3] angiogenesis via alterations in *Vegfa* expression (Figure 9).

Reactive oxygen species (ROS) are the products of physiological aerobic metabolism that can be harmful to cells, tissues, and organs. The skin is affected not only by ROS originating from internal insults but also by external environmental factors such as sun exposure that lead to ROS generation and oxidative stress formation, whereas under some circumstances, for example, skin cancer or the aging process, ROS are harmful; for proper skin wound healing, oxygen-dependent redox signals are required. Hydrogen peroxide and superoxide act as intracellular messengers regulating each of the wound healing phases: inflammation, proliferation, and angiogenesis. However, the disruption of the delicate balance in proper levels of ROS (e.g., excessive ROS accumulation) may impair the skin wound healing process and cause chronic wounds.[58] The principal source of ROS in cells is mitochondria. The electron transport chain (ETC) formed in mitochondria by protein complexes I–IV generates energy via redox reactions that drive the synthesis of ATP.[59]

The proteomic analysis of keratinocytes in our study showed that Foxn1 regulates elements of ETC protein complexes I and III and participates in antioxidant protection through synchronization of the Txn system. Within complex I, we detected upregulation of the expression of Ndufv2, Ndufa2, and Ndufa13, the proteins that are encoded by nuclear DNA.[59] These proteins have to be imported across the mitochondrial membranes to perform their role. Interestingly, in our previous study, we detected upregulation of the expression of voltage-dependent anion-selective channel protein 1 (Vdac1) upon Foxn1 stimulation (in vitro study;[57]) and high levels of *Vdac* mRNA expression in the skin of the Foxn1$^{+/+}$ but not Foxn1$^{-/-}$ mice.[21] Since Vdac1 forms a channel through the mitochondrial outer membrane and the plasma membrane that allows diffusion of small hydrophilic molecules, it is conceivable that Foxn1 controls the process participating in the ETC.

In mitochondria, the dominant ROS buffering (antioxidant) systems include glutaredoxins (Grxs), glutathione

---

FIGURE 8 Hypoxia and Foxn1 regulate skin angiogenesis. (A) Levels of Vegfa and Amotl2 proteins (LC–MS/MS) in keratinocytes transduced with Ad-Foxn1 that were cultured under hypoxic or normoxic conditions. (B) *Vegfa* mRNA expression levels in non-transduced keratinocytes from the Foxn1$^{+/+}$ mice and keratinocytes from the Foxn1$^{-/-}$ mice that were transduced with Ad-Foxn1 or Ad-GFP. Keratinocytes were cultured for 24 h under hypoxia or normoxia. (C) *Vegfa* mRNA expression levels in uninjured (Day 0) and injured (Days 1–21) skin of the Foxn1$^{-/-}$ and Foxn1$^{+/+}$ mice ($n = 6$ skin samples per group/per time point). (D–F) Representative photos of endothelial cell tube formation. HUVECs were cultured in Nor-Foxn1, Hyp-Foxn1, Nor-GFP, Hyp-GFP or control KCM media. Tube formation analysis at 6 h (D′), 12 h (E′), and 18 h (F′) of culture demonstrated small (red), medium (green), and large (yellow) loops. The results are shown as the mean ± SD. The asterisks indicate significant differences in loop number between specific media (*$p < .05$; **$p < .01$). HUVECs, human umbilical vein endothelial cells; KCM conditioned medium collected from keratinocytes; Nor-Foxn1/GFP or Hyp-Foxn1/GFP- transduced by Foxn1 or GFP exposed to normoxia (Nor) or hypoxia (Hyp).

(A)

(B)
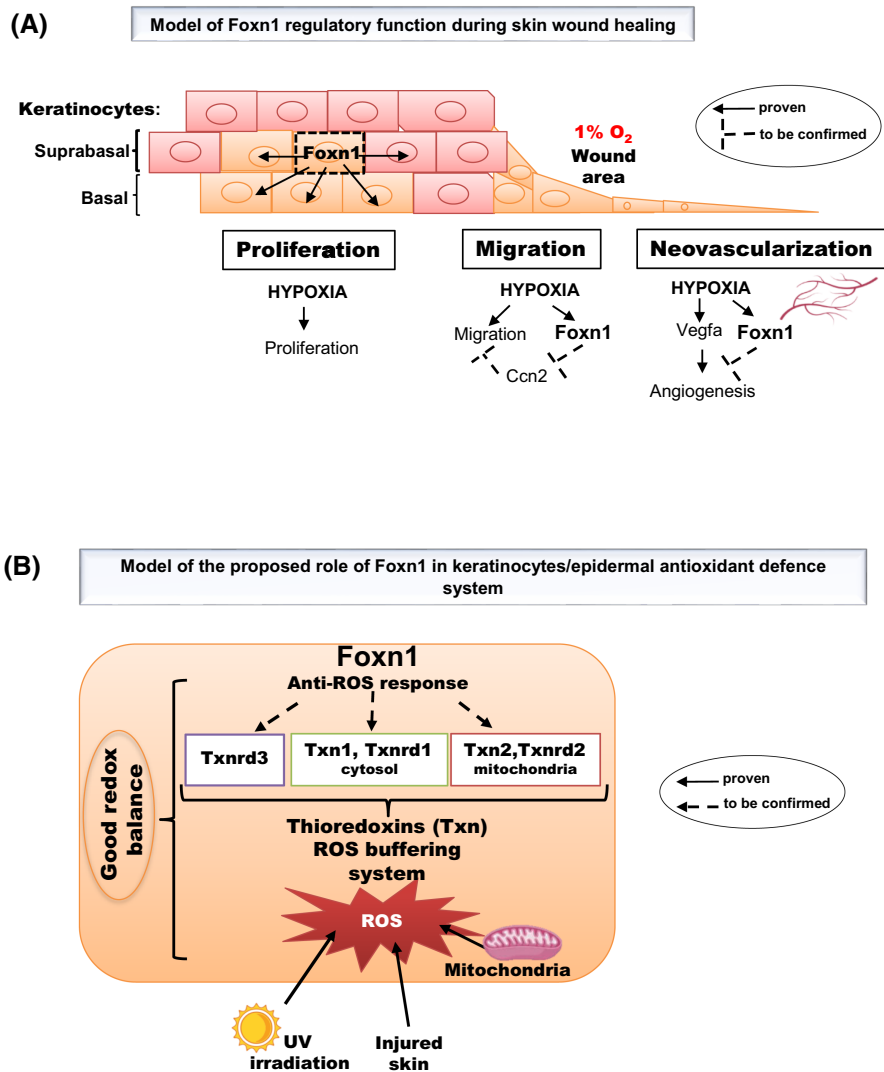
FIGURE 9 Scheme of the proposed role of Foxn1: (A) Model of Foxn1 regulatory function during skin wound healing; (B) Model of the proposed role of Foxn1 in keratinocytes/epidermal antioxidant defense system.

(GSH), peroxyredoxin (Prx), and Txn. The reduction of hydrogen peroxide occurs with the participation of the GSH redox systems, which contain glutathione reductases, peroxidases (Gpx; glutathione peroxidase), and Prx. The activity of Prxs is restored/maintained by sulfiredoxins (Srxn1), endogenous antioxidant proteins inhibiting apoptosis and ROS production.[60] Our proteomic analysis identified Foxn1 as a potent regulator of the Srxn1 protein in keratinocytes regardless of hypoxic or normoxic conditions, thus showing the active participation of Foxn1 in redox processes. However, Txn proteins that are involved in protection against oxidative stress are considered the strongest oxidoreduction system.[61] The potential role of Foxn1 in Txn system regulation was already examined in our previous study, which showed the presence of an active form of Txn in Foxn1-stimulated keratinocytes (in vitro study,[57]) and during the skin wound healing process in Foxn1$^{+/+}$ mice (in vivo study,[45]). Herein, a detailed proteomic analysis of Foxn1-stimulated keratinocytes allowed us to construct protein interaction networks (see Figure 3). Based on the functional protein association

network (STRING database; see Figure 3), which indicated that Foxn1 strongly activates the redox system, we showed that Txn and Txnrd together with detoxification proteins/detox proteins, for example, Nqo1 (quinone dehydrogenase NAD[P]H1), Glrx5 and Sxrn1, form an antioxidant defense coherent system. The results of in vivo experiments from our previous[45] and present study showed that cytosolic isoforms of the Txn system, Txn1, and Txnrd1 are increased in noninjured and injured skin of the Foxn1$^{+/+}$ but not Foxn1$^{-/-}$ mice. However, overexpression of Foxn1 in keratinocytes as well as hypoxic culture conditions did not affect the mRNA or protein levels of Txn1 or Txnrd1 in vitro, suggesting wide-ranging action of Foxn1 in the skin beyond keratinocytes.

In contrast, Txn2, the mitochondrial isoform, together with Txnrd3 proteins, is stimulated by Foxn1 overexpression, particularly under hypoxic conditions. Txn2 plays important roles in the regulation of the mitochondrial membrane potential and in protection against oxidant-induced apoptosis.[62] However, the most intriguing results of our present investigation are the data related to Txnrd3

presence and regulation. Txnrd3 could not only reduce Txn but also oxidize GSH, acting as a strong antioxidant. Initially, the presence of Txnrd3 was specific to the genitals (the testes and ovaries),[36,63] but its expression has also been shown in the spleen, kidney, heart, and liver.[63] Interestingly, our current proteomic analysis of proteins extracted from the Ad-Foxn1-transduced keratinocytes revealed high protein levels of Txnrd3, particularly under hypoxic conditions. This finding was further confirmed by the analysis of *Txnrd3* mRNA expression in the Foxn1-transduced keratinocytes. This is quite an intriguing result considering that the presence of Txnrd3 has been detected in human, canine, and chimpanzee cells thus far, but no active form of Txnrd3 has been found in rats or mice.[36,63] Such surprising data prompted us to verify the levels of *Txnrd3* mRNA in the skin of the Foxn1$^{+/+}$ and Foxn1$^{-/-}$ mice during the skin wound healing process. Our data confirmed the in vitro results, also showing high levels of *Txnrd3* mRNA in the skin of the Foxn1$^{+/+}$ mice with both uninjured and injured skin tissues. These data may indicate the direct involvement of Foxn1 in the activation of Txnrd3 in both keratinocytes (in vitro) and during the skin wound healing process (in vivo) in mice (see Figure 9).

Our initial in silico analysis of the promoter region of the mouse thioredoxin system-related genes has shown that it contains putative FOXN1 binding sites for Txn1 three complete and 31 partial; Txnrd1 one complete and 10 partial; Txn2 two complete and 14 partial; Txnrd2 one complete and 28 partial and for Txnrd3 nine partial (Figure S6). This analysis warrants our further experiments.

Another important aspect in skin wound healing is oxygen tension, which is a crucial microenvironmental factor that influences the development and functioning of the epidermis. After injury, high oxygen consumption and vascular damage lead to partial hypoxia.[64] Lack of oxygen activates Hif-1α, which is involved in all stages of healing: migration and proliferation of keratinocytes and fibroblasts and release of cytokines. Our previous data identified an increase in the mRNA and protein expression of Hif-1α in the skin of the Foxn1$^{+/+}$ versus Foxn1$^{-/-}$ mice during the skin wound healing process.[45] Then, using an in vitro approach, we showed that Foxn1 can act as a potential regulator of Hif-1α, inhibiting its expression under normoxic but not hypoxic conditions.[45] Current proteomic analysis of keratinocytes transduced with Foxn1 under hypoxia identified an increase in Ep300 (p300/CPB) (0.67-fold) protein expression, which is considered a potent coactivator of Hif-1α.[25] Using an in vitro and in vivo approach, we confirmed the increase in *Ep300* mRNA expression in the Ad-Foxn1-stimulated keratinocytes as well as in the wounded skin of the Foxn1$^{+/+}$ mice. These results strongly correlate with the high levels of *Hif-1α*

expression in the skin of Foxn1$^{+/+}$ mice,[45] indicating the possible role of Foxn1 and hypoxia in Hif-1α transcription through Ep300 activation.

The essential aspect of skin wound closure is the migration of keratinocytes, which is affected by the hypoxic environment at the site of the injury.[65,66] However, the mechanism underlying the acceleration of migration under hypoxic conditions is still unclear. Based on the functional analysis (in vitro wound healing scratch), we confirmed previous reports[67,68] showing that the migration of keratinocytes is induced by reduced oxygen availability (hypoxia). However, the results of the present research indicate a directing role of the transcription factor Foxn1 in the regulation of migration. Whereas hypoxia as a single variable induces the migration of keratinocytes, the addition of Ad-Foxn1 to keratinocytes under hypoxia significantly slowed the migration rate. In contrast, overexpression of Foxn1 under normoxic conditions accelerated keratinocyte migration. Furthermore, we identified a group of proteins potentially involved in migration and proliferation. Our attention was drawn to the group of Ccn proteins, particularly Ccn1 and Ccn2, whose levels were significantly reduced in the Foxn1-transduced keratinocytes under both hypoxic and normoxic conditions. The CCN family is involved in many functional features of cells, including migration and proliferation.[39] Many studies have shown the involvement of CCN proteins in the reconstruction of the epidermis after injury; for example, Du et al. showed that CCN1 can directly stimulate re-epithelialization during wound healing.[69] Moreover, data by Kiwanuka et al. showed that CCN2 is transiently expressed by hyperproliferative keratinocytes during full-thickness wound re-epithelialization.[7] However, despite many reports, the expression of CCN in keratinocytes remains controversial. Quan's studies have shown the expression of *CCN2* mRNA in the human epidermis in vivo.[70] In contrast, Rittie et al. showed that CCN2 is not expressed in interfollicular epidermal keratinocytes.[71] Our proteomic data revealed that transduction of keratinocytes by Foxn1 strongly decreased the expression of Ccn1 and Ccn2 proteins regardless of aerobic conditions. Going one step further, we assessed Ccn2 protein levels in the skin of the Foxn1$^{+/+}$ and Foxn1$^{-/-}$ mice during the wound healing process (in vivo). Uninjured skin showed similar Ccn2 protein levels for both the Foxn1$^{+/+}$ and Foxn1$^{-/-}$ mice. However, skin injury resulted in different regulation of Ccn2 levels between the Foxn1$^{+/+}$ and Foxn1$^{-/-}$ mice. Ccn2 protein levels in the skin of the Foxn1$^{+/+}$ mice were stable and unchanged during the wound repair process. Foxn1$^{-/-}$ mice responded to injury with decreased levels of Ccn2 protein at post-wounding days 3–5. These findings, together with the previous study where we

showed that hypoxia induces Foxn1 expression in keratinocytes,[57] may indicate the new signaling pathway in which post-injured skin hypoxia increases Foxn1, resulting in lowered Ccn levels, thereby affecting keratinocyte migration (see Figure 9A). The functional cluster also includes YAP proteins that are upregulated upon Ad-Foxn1 stimulation, regardless of hypoxia or normoxia conditions (see Figure 3). A recent study by Mascharak et al. showed that YAP promotes scar-forming skin healing by driving mechanoresponsive ENFs' (Engrailed-1 lineage-negative fibroblasts) transition to fibrotic EPFs (Engrailed-1 lineage-positive fibroblasts).[72] Whether the capacity for skin wound regeneration observed in Foxn1-deficient mice is related to disruption of Foxn1-YAP signaling can be a foundation for future study.

Angiogenesis is critical for wound healing. Under physiological conditions, angiogenesis in the epidermis is almost absent.[73] However, keratinocytes can release stimulating factors/proteins influencing the deeper layers of the skin, for example, the dermis affecting the angiogenic process. Studies carried out by Wisniewska et al. indicated a proangiogenic effect of hypoxic medium (CM-Hyp) on HUVEC tube formation.[74] Our current proteomic analysis showed a decrease in the levels of Vegfa protein in the Foxn1-induced keratinocytes cultured under hypoxic conditions. Administration of Foxn1-stimulated KCM to HUVECs reduced their proangiogenic potential compared to that of the control media. These results indicate that KCMs release angiogenesis-stimulating factors; however, media collected from the Foxn1-overexpressing keratinocytes interfere with this process (Figure 8D–F, see Figure 9A).

Collectively, the data presented herein identified Foxn1 as a stimulatory element affected by environmental conditions in skin antioxidant defense (Figure 9B) and as a regulator of keratinocyte migration and angiogenesis (Figure 9A). Our findings highlight the newly defined role of Foxn1 as an important regulator in the anti-ROS response through regulation of the Txn system. Moreover, the present data emphasize the role of Foxn1 in the control of complexes I and III of the mitochondrial ETC in keratinocytes. It is well established that oxidative stress in the skin plays a major role in the aging process, which is at least in part caused by age-weakened skin-specific antioxidative mechanisms.[1] Given that most of the antioxidants showed a higher concentration in the epidermis than in the dermis, our data identify Foxn1 as a new component of the system. Moreover, the skin of young and adult Foxn1$^{-/-}$ mice shows features characteristic of aged skin, such as dryness, wrinkling, hair loss, epidermal hyperplasia and altered expression of matrix metalloproteinases, and tissue inhibitors of metalloproteinases.[20,75,76] Intriguingly, all these features are also common in mt-DNA-depleted mice, defining mitochondrial function in skin-associated aging.[77]

Interestingly, Foxn1 expression is limited to two major locations: the epidermis of the skin and the epithelium of the thymus. Age-related thymic involution is implicated as a direct result of diminished expression of Foxn1 in thymic epithelial cells.[78] Reconstruction of Foxn1 expression in the thymus through conditional enhancement of its function regenerated involuted thymus with regard to gene expression profiles and functions similar to those of the juvenile organ.[78] Future studies aiming to restore Foxn1 and its regulatory pathway in the skin of older individuals may provide new solutions for antioxidative skin protection and improvement of skin wound healing.

AUTHOR CONTRIBUTIONS

ACKNOWLEDGMENTS

DISCLOSURES

The authors declare that they have no conflict of interest.

DATA AVAILABILITY STATEMENT

The mass spectrometry data have been deposited to Proteomics Identifications Database (PRIDE) with the dataset identifier PXD031125.

ORCID

Sylwia Machcinska https://orcid.org/0000-0003-3892-4519
Katarzyna Walendzik https://orcid.org/0000-0001-8349-6387

Marta Kopcewicz � https://orcid.
org/0000-0002-9776-4941
Joanna Wisniewska 🔵 https://orcid.
org/0000-0001-5887-450X
Mariola Slowinska 🔵 https://orcid.
org/0000-0002-4366-9535
Barbara Gawronska-Kozak 🔵 https://orcid.
org/0000-0002-2006-8534

REFERENCES

1. Rinnerthaler M, Bischof J, Streubel MK, Trost A, Richter K. Oxidative stress in aging human skin. *Biomolecules*. 2015;5:545-589.

2. Piipponen M, Li D, Landen NX. The immune functions of keratinocytes in skin wound healing. *Int J Mol Sci*. 2020;21:8790.

3. Landen NX, Li D, Stahle M. Transition from inflammation to proliferation: a critical step during wound healing. *Cell Mol Life Sci*. 2016;73:3861-3885.

4. Telorack M, Meyer M, Ingold I, Conrad M, Bloch W, Werner S. A glutathione-Nrf2-thioredoxin cross-talk ensures keratinocyte survival and efficient wound repair. *PLoS Genet*. 2016;12:e1005800.

5. Tottoli EM, Dorati R, Genta I, Chiesa E, Pisani S, Conti B. Skin wound healing process and new emerging Technologies for Skin Wound Care and Regeneration. *Pharmaceutics*. 2020;12:735.

6. Gurtner GC, Werner S, Barrandon Y, Longaker MT. Wound repair and regeneration. *Nature*. 2008;453:314-321.

7. Kiwanuka E, Hackl F, Caterson EJ, et al. CCN2 is transiently expressed by keratinocytes during re-epithelialization and regulates keratinocyte migration in vitro by the ras-MEK-ERK signaling pathway. *J Surg Res*. 2013;185:e109-e119.

8. Pastar I, Stojadinovic O, Yin NC, et al. Epithelialization in wound healing: a comprehensive review. *Adv Wound Care (New Rochelle)*. 2014;3:445-464.

9. Ross C, Alston M, Bickenbach JR, Aykin-Burns N. Oxygen tension changes the rate of migration of human skin keratinocytes in an age-related manner. *Exp Dermatol*. 2011;20:58-63.

10. Schafer M, Werner S. Transcriptional control of wound repair. *Annu Rev Cell Dev Biol*. 2007;23:69-92.

11. Bellavia G, Fasanaro P, Melchionna R, Capogrossi MC, Napolitano M. Transcriptional control of skin reepithelialization. *J Dermatol Sci*. 2014;73:3-9.

12. Mori R, Tanaka K, de Kerckhove M, et al. Reduced FOXO1 expression accelerates skin wound healing and attenuates scarring. *Am J Pathol*. 2014;184:2465-2479.

13. Gawronska-Kozak B, Grabowska A, Kur-Piotrowska A, Kopcewicz M. Foxn1 transcription factor regulates wound healing of skin through promoting epithelial-mesenchymal transition. *PLoS One*. 2016;11:e0150635.

14. Kopcewicz MM, Kur-Piotrowska A, Bukowska J, Gimble JM, Gawronska-Kozak B. Foxn1 and Mmp-9 expression in intact skin and during excisional wound repair in young, adult, and old C57Bl/6 mice. *Wound Repair Regen*. 2017;25:248-259.

15. Lee D, Prowse DM, Brissette JL. Association between mouse nude gene expression and the initiation of epithelial terminal differentiation. *Dev Biol*. 1999;208:362-374.

16. Li J, Baxter RM, Weiner L, Goetinck PF, Calautti E, Brissette JL. Foxn1 promotes keratinocyte differentiation by regulating the activity of protein kinase C. *Differentiation*. 2007;75:694-701.

17. Weiner L, Han R, Scicchitano BM, et al. Dedicated epithelial recipient cells determine pigmentation patterns. *Cell*. 2007;130:932-942.

18. Mecklenburg L, Paus R, Halata Z, Bechtold LS, Fleckman P, Sundberg JP. FOXN1 is critical for onycholemmal terminal differentiation in nude (Foxn1) mice. *J Invest Dermatol*. 2004;123:1001-1011.

19. Potter CS, Pruett ND, Kern MJ, et al. The nude mutant gene Foxn1 is a HOXC13 regulatory target during hair follicle and nail differentiation. *J Invest Dermatol*. 2011;131:828-837.

20. Mecklenburg L, Tychsen B, Paus R. Learning from nudity: lessons from the nude phenotype. *Exp Dermatol*. 2005;14:797-810.

21. Kur-Piotrowska A, Kopcewicz M, Kozak LP, Sachadyn P, Grabowska A, Gawronska-Kozak B. Neotenic phenomenon in gene expression in the skin of Foxn1- deficient (nude) mice—a projection for regenerative skin wound healing. *BMC Genomics*. 2017;18:56.

22. Lokmic Z, Musyoka J, Hewitson TD, Darby IA. Hypoxia and hypoxia signaling in tissue repair and fibrosis. *Int Rev Cell Mol Biol*. 2012;296:139-185.

23. Welsh SJ, Bellamy WT, Briehl MM, Powis G. The redox protein thioredoxin-1 (Trx-1) increases hypoxia-inducible factor 1alpha protein expression: Trx-1 overexpression results in increased vascular endothelial growth factor production and enhanced tumor angiogenesis. *Cancer Res*. 2002;62:5089-5095.

24. Xiao H, Gu Z, Wang G, Zhao T. The possible mechanisms underlying the impairment of HIF-1alpha pathway signaling in hyperglycemia and the beneficial effects of certain therapies. *Int J Med Sci*. 2013;10:1412-1421.

25. Kallio PJ, Okamoto K, O'Brien S, et al. Signal transduction in hypoxic cells: inducible nuclear translocation and recruitment of the CBP/p300 coactivator by the hypoxia-inducible factor-1alpha. *EMBO J*. 1998;17:6573-6586.

26. Sano H, Ichioka S, Sekiya N. Influence of oxygen on wound healing dynamics: assessment in a novel wound mouse model under a variable oxygen environment. *PLoS One*. 2012;7:e50212.

27. Kimmel HM, Grant A, Ditata J. The presence of oxygen in wound healing. *Wounds*. 2016;28:264-270.

28. Zhou J, Damdimopoulos AE, Spyrou G, Brune B. Thioredoxin 1 and thioredoxin 2 have opposed regulatory functions on hypoxia-inducible factor-1alpha. *J Biol Chem*. 2007;282:7482-7490.

29. Cao X, He W, Pang Y, Cao Y, Qin A. Redox-dependent and independent effects of thioredoxin interacting protein. *Biol Chem*. 2020;401:1215-1231.

30. Lee S, Kim SM, Lee RT. Thioredoxin and thioredoxin target proteins: from molecular mechanisms to functional significance. *Antioxid Redox Signal*. 2013;18:1165-1207.

31. Karlenius TC, Tonissen KF. Thioredoxin and cancer: a role for thioredoxin in all states of tumor oxygenation. *Cancer*. 2010;2:209-232.

32. Muri J, Heer S, Matsushita M, et al. The thioredoxin-1 system is essential for fueling DNA synthesis during T-cell metabolic reprogramming and proliferation. *Nat Commun*. 2018;9:1851.

33. Huang Q, Zhou HJ, Zhang H, et al. Thioredoxin-2 inhibits mitochondrial reactive oxygen species generation and

apoptosis stress kinase-1 activity to maintain cardiac function. *Circulation*. 2015;131:1082-1097.

34. Dunn LL, Buckle AM, Cooke JP, Ng MK. The emerging role of the thioredoxin system in angiogenesis. *Arterioscler Thromb Vasc Biol*. 2010;30:2089-2098.

35. Yoshihara E, Masaki S, Matsuo Y, Chen Z, Tian H, Yodoi J. Thioredoxin/Txnip: redoxisome, as a redox switch for the pathogenesis of diseases. *Front Immunol*. 2014;4:514.

36. Su D, Novoselov SV, Sun QA, et al. Mammalian selenoprotein thioredoxin-glutathione reductase. Roles in disulfide bond formation and sperm maturation. *J Biol Chem*. 2005;280:26491-26498.

37. Williams DL, Bonilla M, Gladyshev VN, Salinas G. Thioredoxin glutathione reductase-dependent redox networks in platyhelminth parasites. *Antioxid Redox Signal*. 2013;19:735-745.

38. Nordberg J, Arner ES. Reactive oxygen species, antioxidants, and the mammalian thioredoxin system. *Free Radic Biol Med*. 2001;31:1287-1312.

39. Holbourn KP, Acharya KR, Perbal B. The CCN family of proteins: structure-function relationships. *Trends Biochem Sci*. 2008;33:461-473.

40. Li J, Ye L, Owen S, Weeks HP, Zhang Z, Jiang WG. Emerging role of CCN family proteins in tumorigenesis and cancer metastasis (review). *Int J Mol Med*. 2015;36:1451-1463.

41. Alfaro MP, Deskins DL, Wallus M, et al. A physiological role for connective tissue growth factor in early wound healing. *Lab Invest*. 2013;93:81-95.

42. Lau LF. CCN1/CYR61: the very model of a modern matricellular protein. *Cell Mol Life Sci*. 2011;68:3149-3163.

43. Zhang H, Pasolli HA, Fuchs E. Yes-associated protein (YAP) transcriptional coactivator functions in balancing growth and differentiation in skin. *Proc Natl Acad Sci USA*. 2011;108:2270-2275.

44. Sisco M, Kryger ZB, O'Shaughnessy KD, et al. Antisense inhibition of connective tissue growth factor (CTGF/CCN2) mRNA limits hypertrophic scarring without affecting wound healing in vivo. *Wound Repair Regen*. 2008;16:661-673.

45. Machcinska S, Kopcewicz M, Bukowska J, Walendzik K, Gawronska-Kozak B. Impairment of the Hif-1alpha regulatory pathway in Foxn1-deficient (Foxn1^{−/−}) mice affects the skin wound healing process. *FASEB J*. 2021;35:e21289.

46. Mi H, Ebert D, Muruganujan A, et al. PANTHER version 16: a revised family classification, tree-based classification tool, enhancer regions and extensive API. *Nucleic Acids Res*. 2021;49:D394-D403.

47. Raudvere U, Kolberg L, Kuzmin I, et al. G:profiler: a web server for functional enrichment analysis and conversions of gene lists (2019 update). *Nucleic Acids Res*. 2019;47:W191-W198.

48. Kanehisa M, Goto S. KEGG: Kyoto encyclopedia of genes and genomes. *Nucleic Acids Res*. 2000;28:27-30.

49. Kanehisa M, Sato Y, Furumichi M, Morishima K, Tanabe M. New approach for understanding genome variations in KEGG. *Nucleic Acids Res*. 2019;47:D590-D595.

50. Szklarczyk D, Gable AL, Lyon D, et al. STRING v11: protein-protein association networks with increased coverage, supporting functional discovery in genome-wide experimental datasets. *Nucleic Acids Res*. 2019;47:D607-D613.

51. Shannon P, Markiel A, Ozier O, et al. Cytoscape: a software environment for integrated models of biomolecular interaction networks. *Genome Res*. 2003;13:2498-2504.

52. Grant CE, Bailey TL, Noble WS. FIMO: scanning for occurrences of a given motif. *Bioinformatics*. 2011;27:1017-1018.

53. Schlake T, Schorpp M, Nehls M, Boehm T. The nude gene encodes a sequence-specific DNA binding protein with homologs in organisms that lack an anticipatory immune system. *Proc Natl Acad Sci USA*. 1997;94:3842-3847.

54. Dreos R, Ambrosini G, Groux R, Perier RC, Bucher P. The eukaryotic promoter database in its 30th year: focus on non-vertebrate organisms. *Nucleic Acids Res*. 2017;45:D51-D55.

55. Dreos R, Ambrosini G, Perier RC, Bucher P. The eukaryotic promoter database: expansion of EPDnew and new promoter analysis tools. *Nucleic Acids Res*. 2015;43:D92-D96.

56. Walendzik, K., Kopcewicz, M., Bukowska, J., Panasiewicz, G., Szafranska, B., and Gawronska-Kozak, B. (2020) The transcription factor FOXN1 regulates skin adipogenesis and affects susceptibility to diet-induced obesity. *J Invest Dermatol* 140, 1166–1175 e1169, 1166, 1175.e9

57. Kur-Piotrowska A, Bukowska J, Kopcewicz MM, et al. Foxn1 expression in keratinocytes is stimulated by hypoxia: further evidence of its role in skin wound healing. *Sci Rep*. 2018;8:5425.

58. Sanchez MC, Lancel S, Boulanger E, Neviere R. Targeting oxidative stress and mitochondrial dysfunction in the treatment of impaired wound healing: a systematic review. *Antioxidants-Basel*. 2018;7:98.

59. Koopman WJ, Nijtmans LG, Dieteren CE, et al. Mammalian mitochondrial complex I: biogenesis, regulation, and reactive oxygen species generation. *Antioxid Redox Signal*. 2010;12:1431-1470.

60. He J, Ma M, Li D, et al. Sulfiredoxin-1 attenuates injury and inflammation in acute pancreatitis through the ROS/ER stress/cathepsin B axis. *Cell Death Dis*. 2021;12:626.

61. Roussel X, Bechade G, Kriznik A, et al. Evidence for the formation of a covalent thiosulfinate intermediate with peroxiredoxin in the catalytic mechanism of sulfiredoxin. *J Biol Chem*. 2008;283:22371-22382.

62. Damdimopoulos AE, Miranda-Vizuete A, Pelto-Huikko M, Gustafsson JA, Spyrou G. Human mitochondrial thioredoxin. Involvement in mitochondrial membrane potential and cell death. *J Biol Chem*. 2002;277:33249-33257.

63. Rundlof AK, Janard M, Miranda-Vizuete A, Arner ES. Evidence for intriguingly complex transcription of human thioredoxin reductase 1. *Free Radic Biol Med*. 2004;36:641-656.

64. Tang D, Yan T, Zhang J, Jiang X, Zhang D, Huang Y. Notch1 signaling contributes to hypoxia-induced high expression of integrin beta1 in keratinocyte migration. *Sci Rep*. 2017;7:43926.

65. O'Toole EA, Marinkovich MP, Peavey CL, et al. Hypoxia increases human keratinocyte motility on connective tissue. *J Clin Invest*. 1997;100:2881-2891.

66. Xia YP, Zhao Y, Tyrone JW, Chen A, Mustoe TA. Differential activation of migration by hypoxia in keratinocytes isolated from donors of increasing age: implication for chronic wounds in the elderly. *J Invest Dermatol*. 2001;116:50-56.

67. Cowburn AS, Alexander LEC, Southwood M, Nizet V, Chilvers ER, Johnson RS. Epidermal deletion of HIF-2alpha stimulates wound closure. *J Invest Dermatol*. 2014;134:801-808.

68. Guo S, Dipietro LA. Factors affecting wound healing. *J Dent Res*. 2010;89:219-229.

69. Du H, Zhou Y, Suo Y, et al. CCN1 accelerates re-epithelialization by promoting keratinocyte migration and proliferation during cutaneous wound healing. *Biochem Biophys Res Commun*. 2018;505:966-972.

70. Quan T, Shin S, Qin Z, Fisher GJ. Expression of CCN family of genes in human skin in vivo and alterations by solar-simulated ultraviolet irradiation. *J Cell Commun Signal.* 2009;3:19-23.

71. Rittie L, Perbal B, Castellot JJ Jr, Orringer JS, Voorhees JJ, Fisher GJ. Spatial-temporal modulation of CCN proteins during wound healing in human skin in vivo. *J Cell Commun Signal.* 2011;5:69-80.

72. Mascharak S, DesJardins-Park HE, Davitt MF, et al. Preventing Engrailed-1 activation in fibroblasts yields wound regeneration without scarring. *Science.* 2021;372:eaba2374.

73. Weninger W, Uthman A, Pammer J, et al. Vascular endothelial growth factor production in normal epidermis and in benign and malignant epithelial skin tumors. *Lab Invest.* 1996;75:647-657.

74. Wisniewska J, Slyszewska M, Stalanowska K, et al. Effect of pig-adipose-derived stem Cells' conditioned media on skin wound-healing characteristics in vitro. *Int J Mol Sci.* 2021;22:5469.

75. Prowse DM, Lee D, Weiner L, et al. Ectopic expression of the nude gene induces hyperproliferation and defects in differentiation: implications for the self-renewal of cutaneous epithelia. *Dev Biol.* 1999;212:54-67.

76. Gawronska-Kozak B. Scarless skin wound healing in FOXN1 deficient (nude) mice is associated with distinctive matrix metalloproteinase expression. *Matrix Biol.* 2011;30:290-300.

77. Singh B, Schoeb TR, Bajpai P, Slominski A, Singh KK. Reversing wrinkled skin and hair loss in mice by restoring mitochondrial function. *Cell Death Dis.* 2018;9:735.

78. Bredenkamp N, Nowell CS, Blackburn CC. Regeneration of the aged thymus by a single transcription factor. *Development.* 2014;141:1627-1637.

SUPPORTING INFORMATION

Additional supporting information can be found online in the Supporting Information section at the end of this article.